

**INCLUSIVE HADRONIC DISTRIBUTIONS INSIDE ONE JET AT HIGH ENERGY COLLIDERS
AT “MODIFIED LEADING LOGARITHMIC APPROXIMATION”
OF QUANTUM CHROMODYNAMICS**

R. Perez-Ramos ¹ & B. Machet ²

Laboratoire de Physique Théorique et Hautes Energies ³

Unité Mixte de Recherche UMR 7589

Université Pierre et Marie Curie-Paris6; CNRS; Université Denis Diderot-Paris7

Abstract: After demonstrating their general expressions valid at all x , double differential 1-particle inclusive distributions inside a quark and a gluon jet produced in a hard process, together with the inclusive k_\perp distributions, are calculated at small x in the Modified Leading Logarithmic Approximation (MLLA), as functions of the transverse momentum k_\perp of the outgoing hadron. Results are compared with the Double Logarithmic Approximation (DLA) and a naive DLA-inspired evaluation; sizable corrections are exhibited, which, associated with the requirement to stay in a perturbative regime, set the limits of the interval where our calculations can be trusted. We give predictions for the LHC and Tevatron colliders.

Keywords: *perturbative Quantum Chromodynamics, jets, high-energy colliders*



¹E-mail: perez@lpthe.jussieu.fr

²E-mail: machet@lpthe.jussieu.fr

³LPTHE, tour 24-25, 5^{ème} étage, Université P. et M. Curie, BP 126, 4 place Jussieu, F-75252 Paris Cedex 05 (France)

1 INTRODUCTION

In high energy collisions, perturbative Quantum Chromodynamics (pQCD) successfully predicts inclusive energy spectra of particles in jets. They have been determined within the Modified Leading Logarithmic Approximation (MLLA) [1] [2] as functions of the logarithm of the energy ($\ln(1/x)$) and the result is in nice agreement with the data of $-e^+e^-$ and hadronic – colliders and of deep inelastic scattering (DIS) (see for example [3] [4] [5]). Though theoretical predictions have been derived for small x (energy fraction of one parton inside the jet, $x \ll 1$)⁴, the agreement turns out to hold even for $x \sim 1$. The shape of the inclusive spectrum can even be successfully described by setting the infrared transverse momentum cutoff Q_0 as low as the intrinsic QCD scale Λ_{QCD} (this is the so-called “limiting spectrum”).

This work concerns the production of two hadrons inside a high energy jet (quark or gluon); they hadronize out of two partons at the end of a cascading process that we calculate in pQCD; considering this transition as a “soft” process is the essence of the “Local Parton Hadron Duality” (LPHD) hypothesis [1] [6] [7], that experimental data have, up to now, not put in jeopardy.

More specifically, we study, in the MLLA scheme of resummation, the double differential inclusive 1-particle distribution and the inclusive k_\perp distribution as functions of the transverse momentum of the emitted hadrons; they have up to now only been investigated in DLA (Double Logarithmic Approximation) [1]. After giving general expressions valid at all x , we are concerned in the rest of the paper with the small x region (the range of which is extensively discussed) where explicit analytical formulæ can be obtained; we furthermore consider the limit $Q_0 \approx \Lambda_{QCD}$, which leads to tractable results. We deal with jets of small aperture; as far as hadronic colliders are concerned, this has in particular the advantage to avoid interferences between ingoing and outgoing states.

The paper is organized as follows:

- The description of the process, the notations and conventions are presented in section 2. We set there the general formula of the inclusive 2-particle differential cross section for the production of two hadrons h_1 and h_2 at angle Θ within a jet of opening angle Θ_0 , carrying respectively the fractions x_1 and x_2 of the jet energy E ; the axis of the jet is identified with the direction of the energy flow.
- In section 3, we determine the double differential inclusive 1-particle distribution $\frac{d^2N}{d\ln(1/x_1)d\ln\Theta}$ for the hadron h_1 emitted with the energy fraction x_1 of the jet energy E , at an angle Θ with respect to the jet axis. This expression is valid for all x ; it however only simplifies for $x \ll 1$, where an analytical expression can be obtained; this concerns the rest of the paper.
- In section 4, we go to the small x region and determine $\frac{d^2N}{d\ln(1/x_1)d\ln\Theta}$, $x_1 \ll 1$ both for a gluon jet and for a quark jet. It is plotted as a function of $\ln k_\perp$ (or $\ln\Theta$) for different values of $\ell_1 = \ln(1/x_1)$; the role of the opening angle Θ_0 of the jet is also considered; we compare in particular the MLLA calculation with a naive approach, inspired by DLA calculations, in which furthermore the evolution of the starting jet from Θ_0 , its initial aperture, to the angle Θ between the two outgoing hadrons is not taken into account.

The MLLA expressions of the average gluon and quark color currents $\langle C \rangle_g$ and $\langle C \rangle_q$ involve potentially large corrections with respect to their expressions at leading order; the larger the (small) x domain extends, the larger they are; keeping then under control sets the bound $\ell \equiv \ln \frac{1}{x} \geq 2.5$.

⁴as the exact solution of the MLLA evolution equations

- In section 5, we study the inclusive k_\perp distribution $\frac{dN}{d\ln k_\perp}$, which is the integral of $\frac{d^2N}{dx_1 d\ln \Theta}$ with respect to x_1 ; It is shown in particular how MLLA corrections ensure its positivity. The domain of validity of our predictions is discussed; it is a k_\perp interval, limited by the necessity of staying in the perturbative regime and the range of applicability of our small x approximation; it increases with the jet hardness. The case of mixed gluon and quark jets is evoked.
- A conclusion briefly summarizes the results of this work and comments on its extensions under preparation.

Five appendices complete this work;

- Appendix A is dedicated to the MLLA evolution equation for the partonic fragmentation functions D_g^g or q and their exact solutions [8][9]. They are plotted, together with their derivatives with respect to $\ln(1/x)$ and $\ln k_\perp$. This eases the understanding of the figures in the core of the paper and shows the consistency of our calculations.
- Appendix B presents the explicit expressions at leading order for the average color currents of partons $\langle C \rangle_{A_0}$.
- Appendix C completes section 4 and appendix B by providing explicit formulæ necessary to evaluate the MLLA corrections $\delta \langle C \rangle_{A_0}$ to the average color currents;
- While the core of the paper mainly give results for LHC, Appendix D provides an overview at LEP and Tevatron energies. It is shown how, considering too large values of x ($\ln \frac{1}{x} < 2$) endanger the positivity of $\frac{d^2N}{d\ell d\ln k_\perp}$ at low k_\perp . Curves are also given for $\frac{dN}{d\ln k_\perp}$; the range of applicability of our approximation is discussed in relation with the core of the paper.
- in Appendix E, we compare the DLA and MLLA approximations for the spectrum, the double differential 1-particle inclusive distribution, and the inclusive k_\perp distribution.

2 THE PROCESS UNDER CONSIDERATION

It is depicted in Fig. 1 below. In a hard collision, a parton A_0 is produced, which can be a quark or a gluon⁵. A_0 , by a succession of partonic emissions (quarks, gluons), produces a jet of opening angle Θ_0 , which, in particular, contains the parton A ; A splits into B and C , which hadronize respectively into the two hadrons h_1 and h_2 (and other hadrons). Θ is the angle between B and C .

Because the virtualities of B and C are much smaller than that of A [10], Θ can be considered to be close to the angle between h_1 and h_2 [10][11]; angular ordering is also a necessary condition for this property to hold.

⁵in $p - p$ or $p - \bar{p}$ collisions, two partons collide which can create A_0 either as a quark or as a gluon; in the deep inelastic scattering (DIS) and in e^+e^- colliders, a vector boson (γ or Z) decays into a quark-antiquark pair, and A_0 is a quark (or an antiquark);

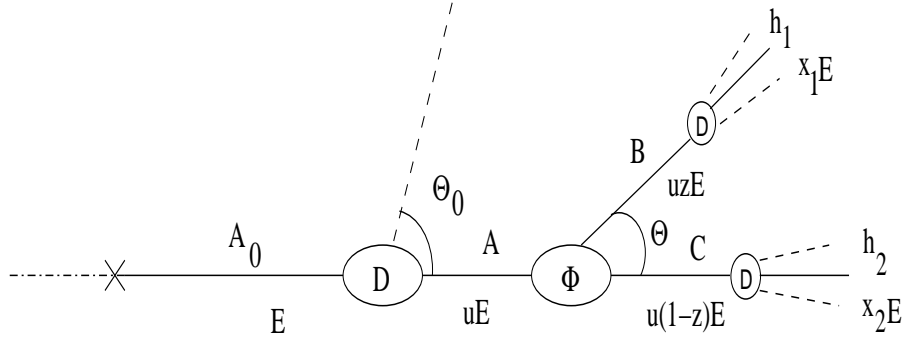


Fig. 1: process under consideration: two hadrons h_1 and h_2 inside one jet.

A_0 carries the energy E . With a probability $D_{A_0}^A$, it gives rise to the (virtual) parton A , which carries the fraction u of the energy E ; $\Phi_A^{BC}(z)$ is the splitting function of A into B and C , carrying respectively the fractions uz and $u(1 - z)$ of E ; h_1 carries the fraction x_1 of E ; h_2 carries the fraction x_2 of E ; $D_B^{h_1} \left(\frac{x_1}{uz}, uzE\Theta, Q_0 \right)$ and $D_C^{h_2} \left(\frac{x_2}{u(1 - z)}, u(1 - z)E\Theta, Q_0 \right)$ are their respective energy distributions. One has $\Theta \leq \Theta_0$. On the other hand, since $k_\perp \geq Q_0$ (Q_0 is the collinear cutoff), the emission angle must satisfy $\Theta \geq \Theta_{min} = Q_0/(xE)$, x being the fraction of the energy E carried away by this particle (see also subsection 2.1 below).

The following expression for the inclusive double differential 2-particle cross section has been demonstrated in [10] [11]:

$$\frac{d\sigma}{d\Omega_{jet} dx_1 dx_2 d\ln \left(\sin^2 \frac{\Theta}{2} \right) \frac{d\varphi}{2\pi}} = \left(\frac{d\sigma}{d\Omega_{jet}} \right)_0 \sum_{A,B,C} \int \frac{du}{u^2} \int dz \left[\frac{1}{z(1-z)} \frac{\alpha_s(k_\perp^2)}{4\pi} \right. \\ \left. \Phi_A^{BC}(z) D_{A_0}^A(u, E\Theta_0, uE\Theta) D_B^{h_1} \left(\frac{x_1}{uz}, uzE\Theta, Q_0 \right) D_C^{h_2} \left(\frac{x_2}{u(1-z)}, u(1-z)E\Theta, Q_0 \right) \right], \quad (1)$$

where $\left(\frac{d\sigma}{d\Omega_{jet}} \right)_0$ is the Born cross section for the production of A_0 , Ω_{jet} is the solid angle of the jet and φ is the azimuthal angle between B and C .

$\alpha_s(q^2)$ is the QCD running coupling constant:

$$\alpha_s(q^2) = \frac{4\pi}{4N_c \beta \ln \frac{q^2}{\Lambda_{QCD}^2}}, \quad (2)$$

where $\Lambda_{QCD} \approx$ a few hundred MeV is the intrinsic scale of QCD and

$$\beta = \frac{1}{4N_c} \left(\frac{11}{3} N_c - \frac{4}{3} T_R \right) \quad (3)$$

is the first term in the perturbative expansion of the β -function, N_c is the number of colors, $T_R = n_f/2$, where n_f is the number of light quark flavors ($n_f = 3$); it is convenient to scale all relevant parameters in units of $4N_c$.

In (1), the integrations over u and z are performed from 0 to 1; the appropriate step functions ensuring $uz \geq x_1$, $u(1 - z) \geq x_2$ (positivity of energy) are included in $D_B^{h_1}$ and $D_C^{h_2}$.

2.1 Notations and variables

The notations and conventions, that are used above and throughout the paper are the following. For any given particle with 4-momentum (k_0, \vec{k}) , transverse momentum $k_\perp \geq Q_0$ (k_\perp is the modulus of the trivector \vec{k}_\perp), carrying the fraction $x = k_0/E$ of the jet energy E , one defines

$$\ell = \ln \frac{E}{k_0} = \ln(1/x), \quad y = \ln \frac{k_\perp}{Q_0}. \quad (4)$$

Q_0 is the infrared cutoff parameter (minimal transverse momentum).

If the radiated parton is emitted with an angle ϑ with respect to the direction of the jet, one has

$$k_\perp = |\vec{k}| \sin \vartheta \approx k_0 \sin \vartheta. \quad (5)$$

The r.h.s. of (5) uses $|\vec{k}| \approx k_0$, resulting from the property that the virtuality k^2 of the emitted parton is negligible in the logarithmic approximation. For collinear emissions ($\vartheta \ll 1$), $k_\perp \sim |\vec{k}| \vartheta \approx k_0 \vartheta$.

One also defines the variable Y_ϑ

$$Y_\vartheta = \ell + y = \ln \left(E \frac{k_\perp}{k_0} \frac{1}{Q_0} \right) \approx \ln \frac{E \vartheta}{Q_0}; \quad (6)$$

to the opening angle Θ_0 of the jet corresponds

$$Y_{\Theta_0} = \ln \frac{E \Theta_0}{Q_0}; \quad (7)$$

$E \Theta_0$ measures the “hardness” of the jet. Since $\vartheta < \Theta_0$, one has the condition, valid for any emitted soft parton off its “parent”

$$Y_\vartheta < Y_{\Theta_0}. \quad (8)$$

The partonic fragmentation function $D_a^b(x_b, Q, q)$ represents the probability of finding the parton b having the fraction x_b of the energy of a inside the dressed parton a ; the virtuality (or transverse momentum) k_a^2 of a can go up to $|Q^2|$, that of b can go down to $|q^2|$.

2.2 The jet axis

The two quantities studied in the following paragraphs (double differential 1-particle inclusive distribution and inclusive k_\perp distribution) refer to the direction (axis) of the jet, with respect to which the angles are measured. We identify it with the direction of the energy flow.

The double differential 1-particle inclusive distribution $\frac{d^2 N}{dx_1 d \ln \Theta}$ is accordingly defined by summing the inclusive double differential 2-particle cross section over all h_2 hadrons and integrating it over their energy fraction x_2 *with a weight which is the energy (x_2) itself*; it measures the angular distribution of an outgoing hadron h_1 with energy fraction x_1 of the jet energy, produced at an angle Θ with respect to the direction of the energy flow.

Once the axis has been fixed, a second (unweighted) integration with respect to the energy of the other hadron (x_1) leads to the inclusive k_\perp distribution $\frac{dN}{d \ln k_\perp}$.

3 DOUBLE DIFFERENTIAL 1-PARTICLE INCLUSIVE DISTRIBUTION $\frac{d^2N}{dx_1 d \ln \Theta}$

After integrating trivially over the azimuthal angle (at this approximation the cross-section does not depend on it), and going to small Θ , the positive quantity $\frac{d^2N}{dx_1 d \ln \Theta}$ reads

$$\frac{d^2N}{dx_1 d \ln \Theta} = \sum_{h_2} \int_0^1 dx_2 x_2 \frac{d\sigma}{d\Omega_{jet} dx_1 dx_2 d \ln \Theta} \frac{1}{\left(\frac{d\sigma}{d\Omega_{jet}} \right)_0}. \quad (9)$$

We use the energy conservation sum rule [12]

$$\sum_h \int_0^1 dx x D_C^h(x, \dots) = 1 \quad (10)$$

expressing that all partons h_2 within a dressed parton (C) carry the total momentum of C , then make the change of variable $v = \frac{x}{u(1-z)}$ where $u(1-z)$ is the upper kinematic limit for x_2 , to get

$$\sum_{h_2} \int_0^{u(1-z)} dx_2 x_2 D_C^{h_2} \left(\frac{x_2}{u(1-z)}, u(1-z)E\Theta, Q_0 \right) = u^2(1-z)^2, \quad (11)$$

and finally obtain the desired quantity;

$$\frac{d^2N}{dx_1 d \ln \Theta} = \sum_{A,B} \int du \int dz \frac{1-z}{z} \frac{\alpha_s(k_\perp^2)}{2\pi} \Phi_A^B(z) D_{A_0}^A(u, E\Theta_0, uE\Theta) D_B^{h_1} \left(\frac{x_1}{uz}, uzE\Theta, Q_0 \right); \quad (12)$$

the summation index C has been suppressed since knowing A and B fixes C .

We can transform (12) by using the following trick:

$$\int du \int \frac{dz}{z} (1-z) = \int du \int \frac{dz}{z} - \int d(uz) \int \frac{du}{u}, \quad (13)$$

and (12) becomes

$$\begin{aligned} \frac{d^2N}{dx_1 d \ln \Theta} &= \sum_A \int du D_{A_0}^A(u, E\Theta_0, uE\Theta) \sum_B \int \frac{dz}{z} \frac{\alpha_s(k_\perp^2)}{2\pi} \Phi_A^B(z) D_B^{h_1} \left(\frac{x_1}{uz}, uzE\Theta, Q_0 \right) \\ &\quad - \sum_B \int d(uz) D_B^{h_1} \left(\frac{x_1}{uz}, uzE\Theta, Q_0 \right) \sum_A \int \frac{du}{u} \frac{\alpha_s(k_\perp^2)}{4\pi} \Phi_A^B \left(\frac{uz}{u} \right) D_{A_0}^A(u, E\Theta_0, uE\Theta). \end{aligned} \quad (14)$$

We then make use of the two complementary DGLAP (see also the beginning of section 4) evolution equations [13] which contain the Sudakov form factors d_A and d_B of the partons A and B respectively:

$$d_A^{-1}(k_A^2) \frac{d}{d \ln k_A^2} \left[d_A(k_A^2) D_A^{h_1} \left(\frac{x_1}{u}, uE\Theta, Q_0 \right) \right] = \frac{\alpha_s(k_\perp^2)}{4\pi} \sum_B \int \frac{dz}{z} \Phi_A^B(z) D_B^{h_1} \left(\frac{x_1}{uz}, uzE\Theta, Q_0 \right), \quad (15)$$

$$d_B(k_B^2) \frac{d}{d \ln k_B^2} \left[d_B^{-1}(k_B^2) D_{A_0}^B(w, E\Theta_0, wE\Theta) \right] = -\frac{\alpha_s(k_\perp^2)}{4\pi} \sum_A \int \frac{du}{u} \Phi_A^B \left(\frac{w}{u} \right) D_{A_0}^A(u, E\Theta_0, uE\Theta); \quad (16)$$

the variable uz occurring in (13) has been introduced; in (15) and (16), $(uE\Theta)^2$ refers respectively to the virtualities k_A^2 and k_B^2 of A and B . Using (15) and (16), (14) transforms into

$$\begin{aligned} \frac{d^2N}{dx_1 d \ln \Theta} &= \sum_A \int du D_{A_0}^A(u, E\Theta_0, uE\Theta) d_A^{-1}(k_A^2) \frac{d}{d \ln k_A^2} \left[d_A(k_A^2) D_A^{h_1} \left(\frac{x_1}{u}, uE\Theta, Q_0 \right) \right] \\ &+ \sum_B \int dw D_B^{h_1} \left(\frac{x_1}{w}, wE\Theta, Q_0 \right) d_B(k_B^2) \frac{d}{d \ln k_B^2} \left[d_B^{-1}(k_B^2) D_{A_0}^B(w, E\Theta_0, wE\Theta) \right]. \end{aligned} \quad (17)$$

$D_A^{h_1}$ depends on the virtuality of A through the variable [1] $\Delta\xi = \xi(k_A^2) - \xi(Q_0^2) = \frac{1}{4N_c\beta} \ln \left(\frac{\ln(k_A^2/\Lambda_{QCD}^2)}{\ln(Q_0^2/\Lambda_{QCD}^2)} \right)$ and elementary kinematic considerations [10] lead to $k_A^2 \sim (uE\Theta)^2$.

By renaming $B \rightarrow A$ and $w \rightarrow u$, (17) finally becomes

$$\begin{aligned} \frac{d^2N}{dx_1 d \ln \Theta} &= \sum_A \int du \left[D_{A_0}^A(u, E\Theta_0, uE\Theta) d_A^{-1}(k_A^2) \frac{d}{d \ln \Theta} \left[d_A(k_A^2) D_A^{h_1} \left(\frac{x_1}{u}, uE\Theta, Q_0 \right) \right] \right. \\ &\quad \left. + D_A^{h_1} \left(\frac{x_1}{u}, uE\Theta, Q_0 \right) d_A(k_A^2) \frac{d}{d \ln \Theta} \left[d_A^{-1}(k_A^2) D_{A_0}^A(u, E\Theta_0, uE\Theta) \right] \right] \\ &= \sum_A \frac{d}{d \ln \Theta} \left[\int du D_{A_0}^A(u, E\Theta_0, uE\Theta) D_A^{h_1} \left(\frac{x_1}{u}, uE\Theta, Q_0 \right) \right], \end{aligned} \quad (18)$$

and one gets

$$\frac{d^2N}{dx_1 d \ln \Theta} = \frac{d}{d \ln \Theta} F_{A_0}^{h_1}(x_1, \Theta, E, \Theta_0) \quad (19)$$

with

$$F_{A_0}^{h_1}(x_1, \Theta, E, \Theta_0) \equiv \sum_A \int du D_{A_0}^A(u, E\Theta_0, uE\Theta) D_A^{h_1} \left(\frac{x_1}{u}, uE\Theta, Q_0 \right); \quad (20)$$

F defined in (20) is the inclusive double differential distribution in x_1 and Θ with respect to the energy flux (the energy fraction of the hadron h_1 within the registered energy flux) and is represented by the convolution of the two functions $D_{A_0}^A$ and $D_A^{h_1}$.

The general formula (19) is valid for all x_1 ; its analytical expression in the small x_1 region will be written in the next section.

4 SOFT APPROXIMATION (SMALL- x_1) FOR $\frac{d^2N}{d\ell_1 d \ln k_\perp}$

At ℓ_1 fixed, since $y_1 = \ln(k_\perp/Q_0)$ and $Y = \ln(E\Theta/Q_0) = \ell_1 + y_1$, $dy_1 = d \ln k_\perp = d \ln \Theta$ and we write hereafter $\frac{d^2N}{d\ell_1 d \ln k_\perp}$ or $\frac{d^2N}{d\ell_1 dy_1}$ instead of $\frac{d^2N}{d\ell_1 d \ln \Theta}$.

Since the u -integral (20) is dominated by $u = \mathcal{O}(1)$ ⁶, the DGLAP [1] partonic distributions $D_{A_0}^A(u, \dots)$ are to be used and, since, on the other hand, we restrict to small x_1 , $x_1/u \ll 1$ and the MLLA inclusive $D_A^{h_1}((x_1/u), \dots)$ are requested. The latter will be taken as the exact solution (see [8]) of the (MLLA)

⁶ $D_A^{h_1} \left(\frac{x_1}{u}, uE\Theta, Q_0 \right) \approx (u/x_1) \times (\text{slowly varying function})$ – see (22) – and the most singular possible behavior of $D_{A_0}^A(u, E\Theta_0, uE\Theta, Q_0)$, which could enhance the contribution of small u , is $\sim 1/u$; however, the integrand then behaves like $\text{Const.} \times (\text{slowly varying function})$ and the contribution of small u to the integral is still negligible.

evolution equations that we briefly sketch out, for the sake of completeness, in appendix A. MLLA evolution equations accounts for the constraints of angular ordering (like DLA but unlike DGLAP equations) and of energy-momentum conservation (unlike DLA).

For soft hadrons, the behavior of the function $D_A^{h_1}(x_1, E\Theta, Q_0)$ at $x_1 \ll 1$ is [1]

$$D_A^{h_1}(x_1, E\Theta, Q_0) \approx \frac{1}{x_1} \rho_A^{h_1} \left(\ln \frac{1}{x_1}, \ln \frac{E\Theta}{Q_0} \equiv Y_\Theta \right), \quad (21)$$

where $\rho_A^{h_1}$ is a slowly varying function of two logarithmic variables that describes the “hump-backed” plateau.

For $D_A^{h_1} \left(\frac{x_1}{u}, uE\Theta, Q_0 \right)$ occurring in (20), this yields

$$D_A^{h_1} \left(\frac{x_1}{u}, uE\Theta, Q_0 \right) \approx \frac{u}{x_1} \rho_A^{h_1} \left(\ln \frac{u}{x_1}, \ln u + Y_\Theta \right). \quad (22)$$

Because of (6), one has

$$\rho_A^h(\ell, Y_\Theta) = \rho_A^{h_1}(\ell, \ell + y) = \tilde{D}_A^h(\ell, y), \quad (23)$$

and, in what follows, we shall always consider the functions

$$x D_A(x, E\Theta, Q_0) = \tilde{D}_A(\ell, y). \quad (24)$$

The expansion of $\rho_A^{h_1} \left(\ln \frac{u}{x_1}, \ln u + Y_\Theta \right)$ around $u = 1$ ($\ln u = \ln 1$) reads

$$\begin{aligned} \frac{x_1}{u} D_A^{h_1} \left(\frac{x_1}{u}, uE\Theta, Q_0 \right) &= \rho_A^{h_1}(\ell_1 + \ln u, Y_\Theta + \ln u) = \rho_A^{h_1}(\ell_1 + \ln u, y_1 + \ell_1 + \ln u) \\ &= \tilde{D}_A^{h_1}(\ell_1 + \ln u, y_1) = \tilde{D}_A^{h_1}(\ell_1, y_1) + \ln u \frac{d}{d\ell_1} \tilde{D}_A^{h_1}(\ell_1, y_1) + \dots, \end{aligned} \quad (25)$$

such that

$$\begin{aligned} x_1 F_{A_0}^{h_1}(x_1, \Theta, E, \Theta_0) &\approx \sum_A \int du u D_{A_0}^A(u, E\Theta_0, uE\Theta) \left(\tilde{D}_A^{h_1}(\ell_1, y_1) + \ln u \frac{d\tilde{D}_A^{h_1}(\ell_1, y_1)}{d\ell_1} \right) \\ &= \sum_A \left[\int du u D_{A_0}^A(u, E\Theta_0, uE\Theta) \right] \tilde{D}_A^{h_1}(\ell_1, y_1) \\ &\quad + \sum_A \left[\int du u \ln u D_{A_0}^A(u, E\Theta_0, uE\Theta) \right] \frac{d\tilde{D}_A^{h_1}(\ell_1, y_1)}{d\ell_1}; \end{aligned} \quad (26)$$

the second line in (26) is the $\mathcal{O}(1)$ main contribution; the third line, which accounts for the derivatives, including the variation of α_s , makes up corrections of relative order $\mathcal{O}(\sqrt{\alpha_s})$ with respect to the leading terms (see also (37)), which have never been considered before; since, in the last line of (26), $u \leq 1 \Rightarrow \ln u \leq 0$ and $\frac{d\tilde{D}_A^{h_1}}{d\ell_1}$ is positive (see appendix A.4), the corresponding correction is negative. A detailed discussion of all corrections is made in subsections 4.1 and 4.4

It is important for further calculations that (20) has now factorized.

While (20) (26) involve (inclusive) *hadronic* fragmentation functions $\tilde{D}_A^{h_1} = \tilde{D}_g^{h_1}$ or $\tilde{D}_q^{h_1}$, the MLLA *partonic* functions $\tilde{D}_A^b(\ell, y)$ satisfy the evolution equations (46) with exact solution (52), demonstrated in [8] and recalled in appendix A. The link between the latter ($\tilde{D}_g^g, \tilde{D}_q^g, \tilde{D}_g^q, \tilde{D}_q^q$) and the former goes as follows. At small x , since quarks are secondary products of gluons, for a given “parent”, the number

of emitted quarks is a universal function of the number of emitted gluons: the upper indices of emitted partons are thus correlated, and we can replace in (26) the inclusive fragmentation functions by the partonic ones, go to the functions $\tilde{D}_A(\ell, y)$, where the upper index (which we will omit) is indifferently g or q , and rewrite

$$x_1 F_{A_0}^{h_1}(x_1, \Theta, E, \Theta_0) \approx \sum_A \left(\langle u \rangle_{A_0}^A + \delta \langle u \rangle_{A_0}^A \psi_{A, \ell_1}(\ell_1, y_1) \right) \tilde{D}_A(\ell_1, y_1), \quad (27)$$

with⁷

$$\begin{aligned} \langle u \rangle_{A_0}^A &= \int_0^1 du u D_{A_0}^A(u, E\Theta_0, uE\Theta) \approx \int_0^1 du u D_{A_0}^A(u, E\Theta_0, E\Theta), \\ \delta \langle u \rangle_{A_0}^A &= \int_0^1 du (u \ln u) D_{A_0}^A(u, E\Theta_0, uE\Theta) \approx \int_0^1 du (u \ln u) D_{A_0}^A(u, E\Theta_0, E\Theta), \end{aligned} \quad (28)$$

and

$$\psi_{A, \ell_1}(\ell_1, y_1) = \frac{1}{\tilde{D}_A(\ell_1, y_1)} \frac{d\tilde{D}_A(\ell_1, y_1)}{d\ell_1}. \quad (29)$$

Thus, for a gluon jet

$$\begin{aligned} x_1 F_g^{h_1}(x_1, \Theta, E, \Theta_0) &\approx \langle u \rangle_g^g \tilde{D}_g(\ell_1, y_1) + \langle u \rangle_g^q \tilde{D}_q(\ell_1, y_1) \\ &+ \delta \langle u \rangle_g^g \psi_{g, \ell_1}(\ell_1, y_1) \tilde{D}_g(\ell_1, y_1) \\ &+ \delta \langle u \rangle_g^q \psi_{q, \ell_1}(\ell_1, y_1) \tilde{D}_q(\ell_1, y_1), \end{aligned} \quad (30)$$

and for a quark jet

$$\begin{aligned} x_1 F_q^{h_1}(x_1, \Theta, E, \Theta_0) &\approx \langle u \rangle_q^g \tilde{D}_g(\ell_1, y_1) + \langle u \rangle_q^q \tilde{D}_q(\ell_1, y_1) \\ &+ \delta \langle u \rangle_q^g \psi_{g, \ell_1}(\ell_1, y_1) \tilde{D}_g(\ell_1, y_1) \\ &+ \delta \langle u \rangle_q^q \psi_{q, \ell_1}(\ell_1, y_1) \tilde{D}_q(\ell_1, y_1). \end{aligned} \quad (31)$$

It turns out (see [1]) that the MLLA corrections to the formulæ

$$\tilde{D}_q^g \approx \frac{C_F}{N_c} \tilde{D}_g^g, \quad \tilde{D}_q^q \approx \frac{C_F}{N_c} \tilde{D}_g^q, \quad (32)$$

do not modify the results and we use (32) in the following. We rewrite accordingly (30) and (31)

$$\begin{aligned} x_1 F_g^{h_1}(x_1, \Theta, E, \Theta_0) &\approx \frac{\langle C \rangle_g^0 + \delta \langle C \rangle_g}{N_c} \tilde{D}_g(\ell_1, y_1) \equiv \frac{\langle C \rangle_g}{N_c} \tilde{D}_g(\ell_1, y_1), \\ x_1 F_q^{h_1}(x_1, \Theta, E, \Theta_0) &\approx \frac{\langle C \rangle_q^0 + \delta \langle C \rangle_q}{N_c} \tilde{D}_g(\ell_1, y_1) \equiv \frac{\langle C \rangle_q}{N_c} \tilde{D}_g(\ell_1, y_1), \end{aligned} \quad (33)$$

with

$$\begin{aligned} \langle C \rangle_g^0 &= \langle u \rangle_g^g N_c + \langle u \rangle_g^q C_F, \\ \langle C \rangle_q^0 &= \langle u \rangle_q^g N_c + \langle u \rangle_q^q C_F, \end{aligned} \quad (34)$$

⁷In (28), u is integrated from 0 to 1, while, kinematically, it cannot get lower than x_1 ; since we are working at small x_1 , this approximation is reasonable.

and where we have called

$$\begin{aligned}\delta \langle C \rangle_g &= N_c \delta \langle u \rangle_g^g \psi_{g,\ell_1}(\ell_1, y_1) + C_F \delta \langle u \rangle_g^q \psi_{q,\ell_1}(\ell_1, y_1), \\ \delta \langle C \rangle_q &= N_c \delta \langle u \rangle_q^g \psi_{g,\ell_1}(\ell_1, y_1) + C_F \delta \langle u \rangle_q^q \psi_{q,\ell_1}(\ell_1, y_1).\end{aligned}\quad (35)$$

$\langle C \rangle_{A_0}$ is the average color current of partons caught by the calorimeter.

Plugging (33) into (19) yields the general formula

$$\left(\frac{d^2 N}{d\ell_1 d \ln k_\perp} \right)_{q,g} = \frac{d}{dy_1} \left[\frac{\langle C \rangle_{q,g}}{N_c} \tilde{D}_g(\ell_1, y_1) \right] \quad (36)$$

The first line of (30) and (31) are the leading terms, the second and third lines are corrections. Their relative order is easily determined by the following relations (see (47) for the definition of γ_0)

$$\begin{aligned}\frac{d^2 N}{d\ell_1 d \ln k_\perp} &= \frac{\langle C \rangle_{q,g}}{N_c} \frac{d}{dy_1} \tilde{D}_g(\ell_1, y_1) + \frac{1}{N_c} \tilde{D}_g(\ell_1, y_1) \frac{d}{dy_1} \langle C \rangle_{q,g}, \\ \frac{d}{dy_1} \tilde{D}_g(\ell_1, y_1) &= \mathcal{O}(\gamma_0) = \mathcal{O}(\sqrt{\alpha_s}), \\ \frac{d}{dy_1} \langle C \rangle_{q,g} &= \mathcal{O}(\gamma_0^2) = \mathcal{O}(\alpha_s);\end{aligned}\quad (37)$$

The different contributions are discussed in subsections 4.1 and 4.4 below.

- $\frac{d\tilde{D}_g(\ell,y)}{d \ln k_\perp} \equiv \frac{d\tilde{D}_g(\ell,y)}{dy}$ (see the beginning of this section) occurring in (36) is plotted in Fig. 12 and 13 of appendix A, and $\frac{d\tilde{D}_g(\ell,y)}{d\ell}$ occurring in (27) (29) is plotted in Figs. 14 and 15.
- The expressions for the leading terms of $x_1 F_{A_0}^{h_1}(x_1, \Theta, E, \Theta_0)$ together with the ones of $\langle C \rangle_g^0$ and $\langle C \rangle_q^0$ are given in appendix B.
- The calculations of $\delta \langle C \rangle_g$ and $\delta \langle C \rangle_q$ are detailed in appendix C, where the explicit analytical expressions for the $\langle u \rangle$'s and $\delta \langle u \rangle$'s are also given.

We call “naive” the approach” in which one disregards the evolution of the jet between Θ_0 and Θ ; this amounts to taking to zero the derivative of $\langle C \rangle_{q,g}$ in (36); (58), (59), (60) then yield

$$\langle C \rangle_g^{naive} = N_c, \quad \langle C \rangle_q^{naive} = C_F. \quad (38)$$

4.1 The average color current $\langle C \rangle_{A_0}$

On Fig. 2 below, we plot, for $Y_{\Theta_0} = 7.5$, $\langle C \rangle_q^0$, $\langle C \rangle_q^0 + \delta \langle C \rangle_q$, $\langle C \rangle_g^0$, $\langle C \rangle_g^0 + \delta \langle C \rangle_g$ as functions of y , for $\ell = 2.5$ on the left and $\ell = 3.5$ on the right. Since $\Theta \leq \Theta_0$, the curves stop at y such that $y + \ell = Y_{\Theta_0}$; they reach then their respective asymptotic values N_c for $\langle C \rangle_g$ and C_F for $\langle C \rangle_q$, at which $\delta \langle C \rangle_q$ and $\delta \langle C \rangle_g$ also vanish (see also the naive approach (38)). These corrections also vanish at $y = 0$ because they are proportional to the logarithmic derivative $(1/\tilde{D}(\ell, y))(d\tilde{D}(\ell, y)/d\ell)$ (see (35)) which both vanish, for q and g , at $y = 0$ (see appendix A, and Figs. 16-17); there, the values of $\langle C \rangle_g$ and $\langle C \rangle_q$ can be determined from (58)(59).

The curves corresponding to LEP and Tevatron working conditions, $Y_{\Theta_0} = 5.2$, are shown in appendix D.

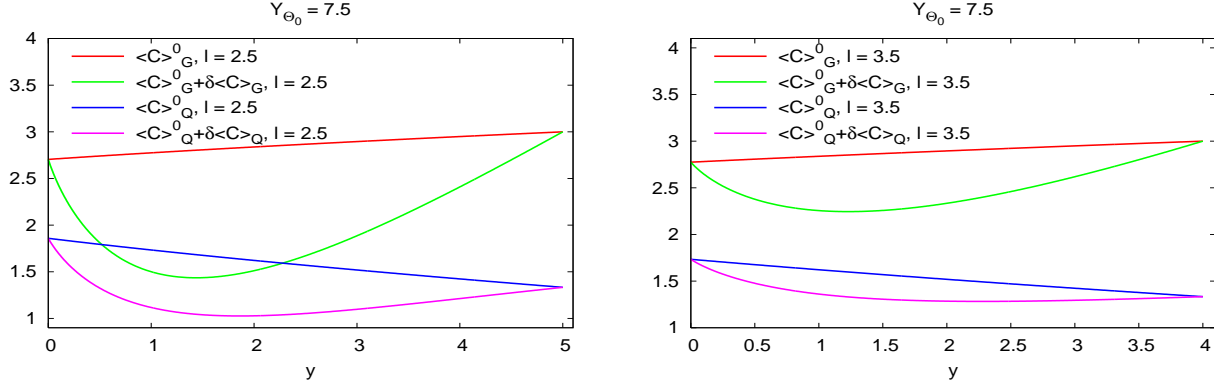


Fig. 2: $\langle C \rangle_{A_0}^0$ and $\langle C \rangle_{A_0}^0 + \delta \langle C \rangle_{A_0}$ for quark and gluon jets, as functions of y , for $Y_{\Theta_0} = 7.5$, $\ell = 2.5$ on the left and $\ell = 3.5$ on the right.

Two types of MLLA corrections arise in our calculation, which are easily visualized on Fig. 2:

- * through the expansion (25) around $u = 1$, the average color current $\langle C \rangle_{A_0}^0$ gets modified by $\delta \langle C \rangle_{A_0} \leq 0$ of relative order $\mathcal{O}(\sqrt{\alpha_s})$; it is represented on Fig. 2 by the vertical difference between the straight lines ($\langle C \rangle_{A_0}^0$) and the curved ones ($\langle C \rangle_{A_0}^0 + \delta \langle C \rangle_{A_0}$);
- * the derivative of $\langle C \rangle_{A_0}^0$ with respect to y is itself of relative order $\mathcal{O}(\sqrt{\alpha_s})$ with respect to that of \tilde{D}_g ; it is the slopes of the straight lines in Fig. 2.

The y derivatives of $\langle C \rangle_{A_0}^0 + \delta \langle C \rangle_{A_0}$ differ from the ones of the leading $\langle C \rangle_{A_0}^0$; this effect combines the two types of MLLA corrections mentioned above: the derivation of $\langle C \rangle$ with respect to y and the existence of $\delta \langle C \rangle$.

For $Y_{\Theta_0} = 7.5$, the $\delta \langle C \rangle$ correction can represent 50% of $\langle C \rangle_g$ at $\ell = 2.5$ and $y \approx 1.5$; for higher values of ℓ (smaller x), as can be seen on the right figure, its importance decreases; it is remarkable that, when $\delta \langle C \rangle$ is large, the corrections to $\frac{d\langle C \rangle}{dy}$ with respect to $\frac{d\langle C \rangle^0}{dy}$ become small, *and vice-versa*: at both extremities of the curves for the color current, the $\delta \langle C \rangle$ corrections vanish, but their slopes are very different from the ones of the straight lines corresponding to $\langle C \rangle^0$.

So, all corrections that we have uncovered are potentially large, even $\frac{d\delta \langle C \rangle}{dy}$, which is the y derivative of a MLLA corrections. This raises the question of the validity of our calculations. Several conditions need to be fulfilled at the same time:

- * one must stay in the perturbative regime, which needs $y_1 \geq 1$ ($k_\perp > 2.72 \Lambda_{QCD} \approx .7 \text{ GeV}$; this condition excludes in particular the zone of very large increase of $\frac{d^2 N}{d \ell_1 d \ln k_\perp}$ when $y_1 \rightarrow 0$ (this property is linked to the divergence of the running coupling constant of QCD $\alpha_s(k_\perp^2) \rightarrow \infty$ when $k_\perp \rightarrow \Lambda_{QCD}$).
- * x must be small, that is ℓ large enough, since this is the limit at which we have obtained analytical results; we see on Fig. 2 that it cannot go reasonably below $\ell = 2.5$; this lower threshold turns out to be of the same order magnitude as the one found in the forthcoming study of 2-particle correlations inside one jet in the MLLA approximation [9];
- * (MLLA) corrections to the leading behavior must stay under control (be small “enough”); if one only looks at the size of the $\delta \langle C \rangle$ corrections at $Y_{\Theta_0} = 7.5$, it would be very tempting to exclude $y \in [.5, 2.5]$; however this is without taking into account the y derivatives of $\langle C \rangle$, which also play an important role, as stressed above; our attitude, which will be confirmed or not by experimental results, is to only globally constrain the overall size of all corrections by setting x small enough.

Would the corrections become excessively large, the expansion (25) should be pushed one step further, which corresponds to next-to-MLLA (NMLLA) corrections; this should then be associated with NMLLA evolution equations for the inclusive spectrum, which lies out of the scope of the present work.

Though $\delta \langle C \rangle$ can be large, specially at small values of ℓ , the positivity of $\langle C \rangle^0 + \delta \langle C \rangle$ is always preserved on the whole allowed range of y .

The difference between the naive and MLLA calculations lies in neglecting or not the evolution of the jet between Θ_0 and Θ , or, in practice, in considering or not the average color current $\langle C \rangle_{A_0}$ as a constant.

We present below our results for a gluon and for a quark jet. We choose two values $Y_{\Theta_0} = 7.5$, which can be associated with the LHC environment⁸, and the unrealistic $Y_{\Theta_0} = 10$ (see appendix D for $Y_{\Theta_0} = 5.2$ and 5.6, corresponding to the LEP and Tevatron working conditions). For each value of Y_{Θ_0} we make the plots for two values of ℓ_1 , and compare one of them with the naive approach.

In the rest of the paper we always consider the limiting case $Q_0 \rightarrow \Lambda_{QCD} \Leftrightarrow \lambda \approx 0$,

$$\lambda = \ln \frac{Q_0}{\Lambda_{QCD}}. \quad (39)$$

The curves stop at their kinematic limit $y_{1\max}$ such that $y_{1\max} + \ell_1 = Y_{\Theta_0}$.

4.2 $\frac{d^2N}{d\ell_1 d \ln k_\perp}$ at small x_1 : gluon jet

On Fig. 3 below is plotted the double differential distribution $\frac{d^2N}{d\ell_1 d \ln k_\perp}$ of a parton inside a gluon jet as a function of y_1 for different values of ℓ_1 (fixed).

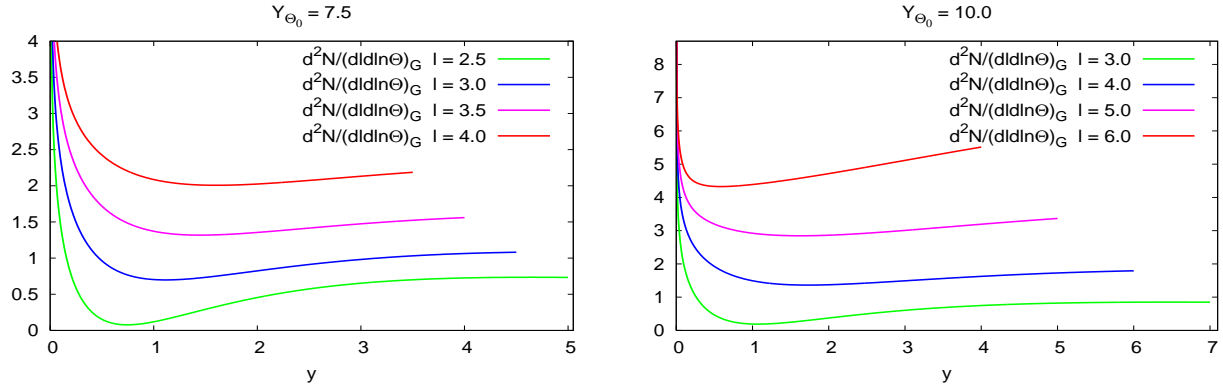


Fig. 3: $\frac{d^2N}{d\ell_1 d \ln k_\perp}$ for a gluon jet.

On Fig. 4 are compared, for a given value of ℓ_1 , the two following cases:

* the first corresponds to the full formulae (33) (36);

⁸Sharing equally the 14 TeV of available center of mass energy between the six constituent partons of the two colliding nucleons yields $E \approx 2.3$ TeV by colliding parton, one considers a jet opening angle of $\Theta \approx .25$ and $Q_0 \approx \Lambda_{QCD} \approx 250$ MeV; this gives $Y = \ln \frac{E\Theta}{Q_0} \approx 7.7$.

* the second corresponds to the naive approach (see the definition above (38))

$$\left(\frac{d^2 N}{d\ell_1 d \ln k_\perp} \right)_g^{naive} = \frac{d}{dy_1} \tilde{D}_g(\ell_1, y_1); \quad (40)$$

$\frac{d\tilde{D}_g(\ell_1, y_1)}{dy_1}$ is given in (56).

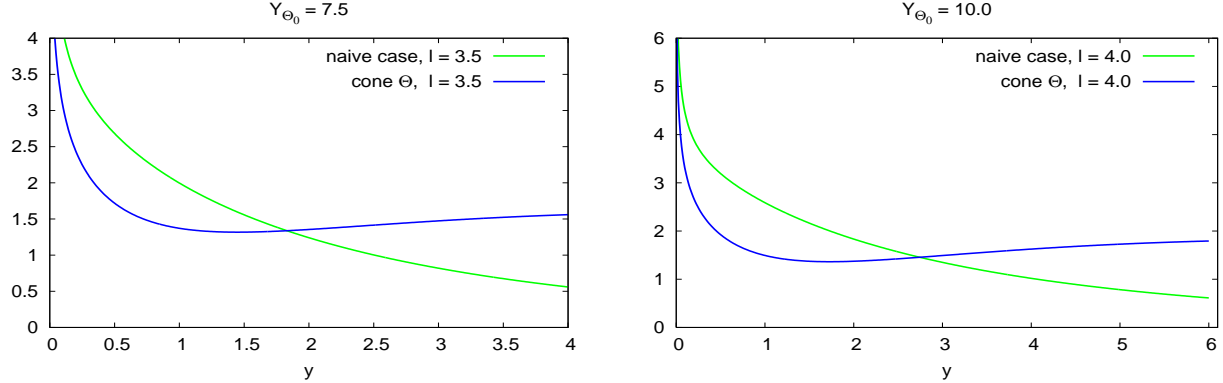


Fig. 4: $\frac{d^2 N}{d\ell_1 d \ln k_\perp}$ for a gluon jet at fixed ℓ_1 , MLLA and naive approach.

The raise of the distribution at large k_\perp is due to the positive corrections already mentioned in the beginning of this section, which arise from the evolution of the jet between Θ and Θ_0 .

4.3 $\frac{d^2 N}{d\ell_1 d \ln k_\perp}$ at small x_1 : quark jet

On Fig. 5 is plotted the double differential distribution $\frac{d^2 N}{d\ell_1 d \ln k_\perp}$ of a parton inside a quark jet as a function of y_1 for different values of ℓ_1 (fixed).

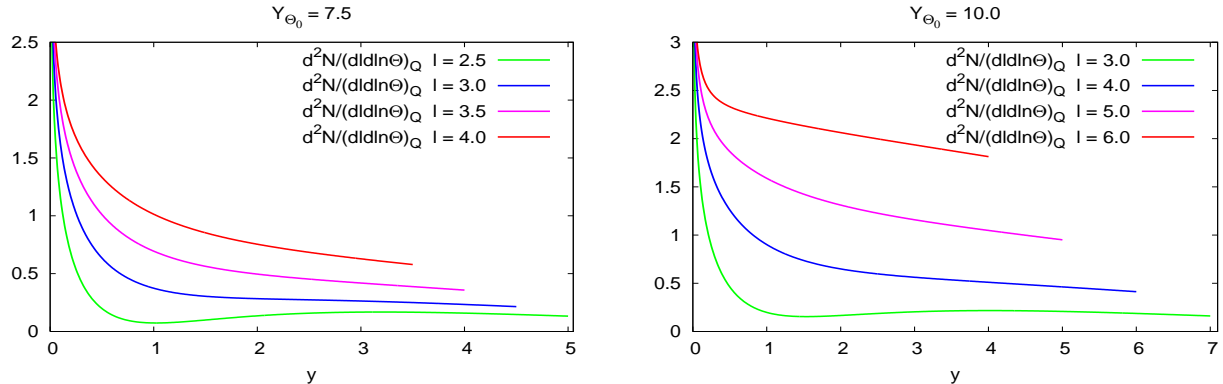


Fig. 5: $\frac{d^2 N}{d\ell_1 d \ln k_\perp}$ for a quark jet.

On Fig. 6 are compared, for a given ℓ_1 fixed, the full formulæ (33) (36) and the naive approach

$$\left(\frac{d^2 N}{d\ell_1 d \ln k_\perp} \right)_q^{naive} = \frac{C_F}{N_c} \frac{d}{dy_1} \tilde{D}_g(\ell_1, y_1). \quad (41)$$

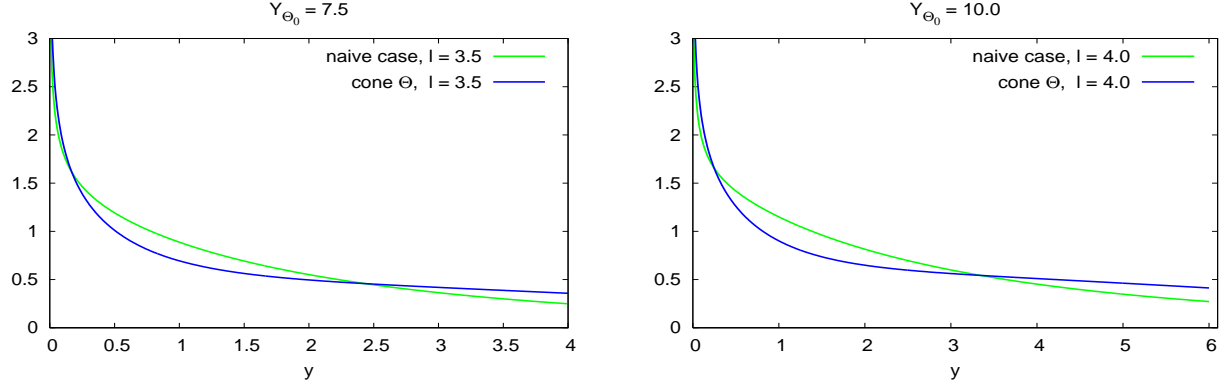


Fig. 6: $\frac{d^2N}{d\ell_1 d \ln k_\perp}$ for a quark jet at fixed ℓ_1 , MLLA and naive approach.

We note, like for gluon jets, at large y , a (smaller) increase of the distribution, due to taking into account the jet evolution between Θ and Θ_0 .

4.4 Comments

The gluon distribution is always larger than the quark distribution; this can also be traced in Fig. 2 which measures in particular the ratio of the color currents $\langle C \rangle_g / \langle C \rangle_q$.

The curves for $\frac{d^2N}{d\ell_1 d \ln k_\perp}$ have been drawn for $\ell_1 \equiv \ln(1/x_1) \geq 2.5$; going below this threshold exposes to excessively large MLLA corrections.

The signs of the two types of MLLA corrections pointed at in subsection 4.1 vary with y : $\delta \langle C \rangle$ always brings a negative correction to $\langle C \rangle^0$, and to $\frac{d^2N}{d\ell_1 d \ln k_\perp}$; for $y \geq 1.5$, the slope of $\langle C \rangle$ is always larger than the one of $\langle C \rangle^0$, while for $y \leq 1.5$ it is the opposite. It is accordingly not surprising that, on Figs. 4 and 6, the relative positions of the curves corresponding to the MLLA calculation and to a naive calculation change with the value of y . At large y , one gets a growing behavior of $\frac{d^2N}{d\ell_1 d \ln k_\perp}$ for gluon jets (Fig. 4), and a slowly decreasing one for quark jets (Fig. 6), which could not have been anticipated *a priori*.

We study in appendix E.2, how MLLA results compare with DLA [14] [15], in which the running of α_s has been “factored out”.

5 INCLUSIVE k_\perp DISTRIBUTION $\frac{dN}{d \ln k_\perp}$

Another quantity of interest is the inclusive k_\perp distribution which is defined by

$$\left(\frac{dN}{d \ln k_\perp} \right)_{g \text{ or } q} = \int dx_1 \left(\frac{d^2N}{dx_1 d \ln k_\perp} \right)_{g \text{ or } q} \equiv \int_{\ell_{min}}^{Y_{\Theta_0} - y} d\ell_1 \left(\frac{d^2N}{d\ell_1 d \ln k_\perp} \right)_{g \text{ or } q} ; \quad (42)$$

it measures the transverse momentum distribution of one particle with respect to the direction of the energy flow (jet axis).

We have introduced in (42) a lower bound of integration ℓ_{min} because our calculations are valid for small x_1 , that is for large ℓ_1 . In a first step we take $\ell_{min} = 0$, then vary it to study the sensitivity of the calculation to the region of large x_1 .

We plot below the inclusive k_\perp distributions for gluon and quark jets, for the same two values $Y_{\Theta_0} = 7.5$ and $Y_{\Theta_0} = 10$ as above, and compare them, on the same graphs, with the “naive calculations” of the same quantity.

5.1 Gluon jet; $\ell_{min} = 0$

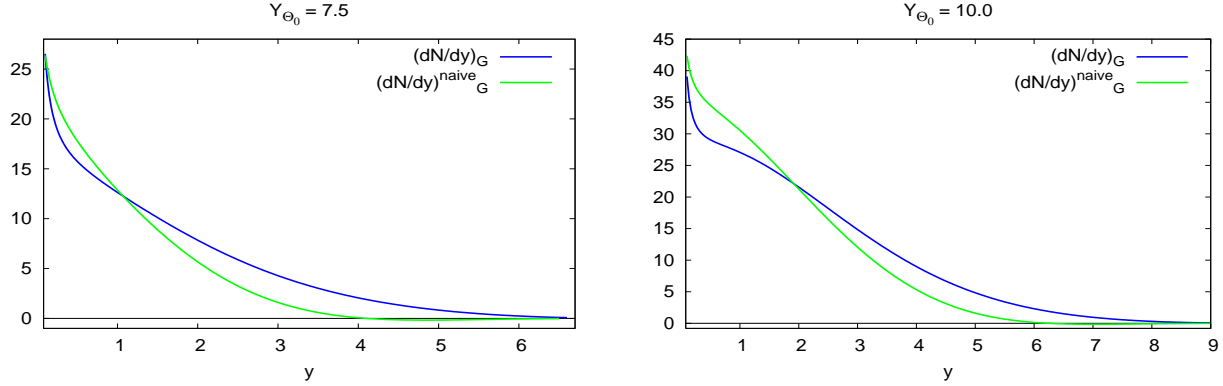


Fig. 7: $\frac{dN}{d\ln k_\perp}$ for a gluon jet, MLLA and naive approach, for $\ell_{min}=0$, $Y_{\Theta_0} = 7.5$ and $Y_{\Theta_0} = 10$.

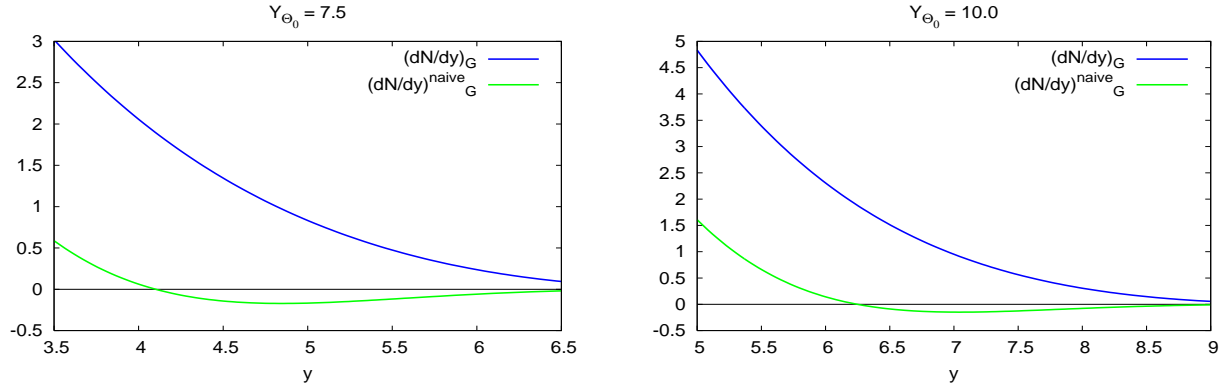


Fig. 8: enlargements of Fig. 7 at large k_\perp

5.2 Quark jet; $\ell_{min} = 0$

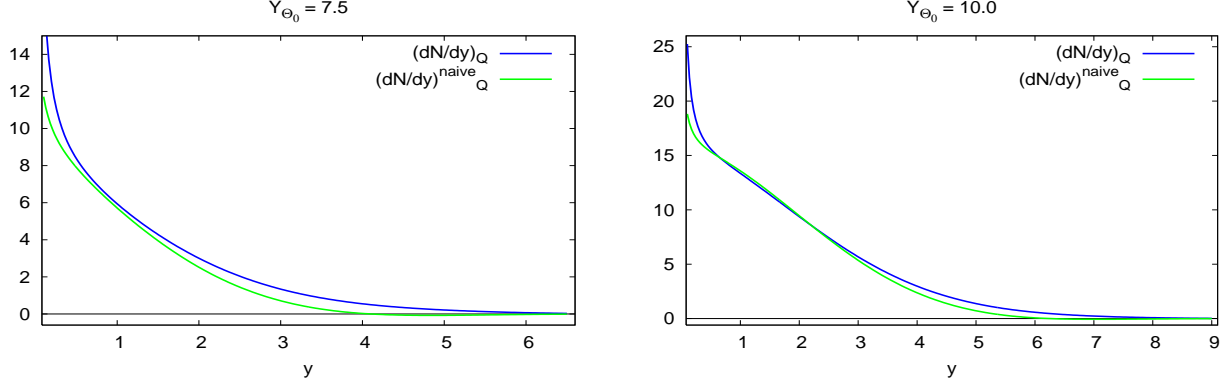


Fig. 9: $\frac{dN}{d\ln k_\perp}$ for a quark jet, MLLA and naive approach, for $\ell_{min}=0$, $Y_{\Theta_0} = 7.5$ and $Y_{\Theta_0} = 10$.

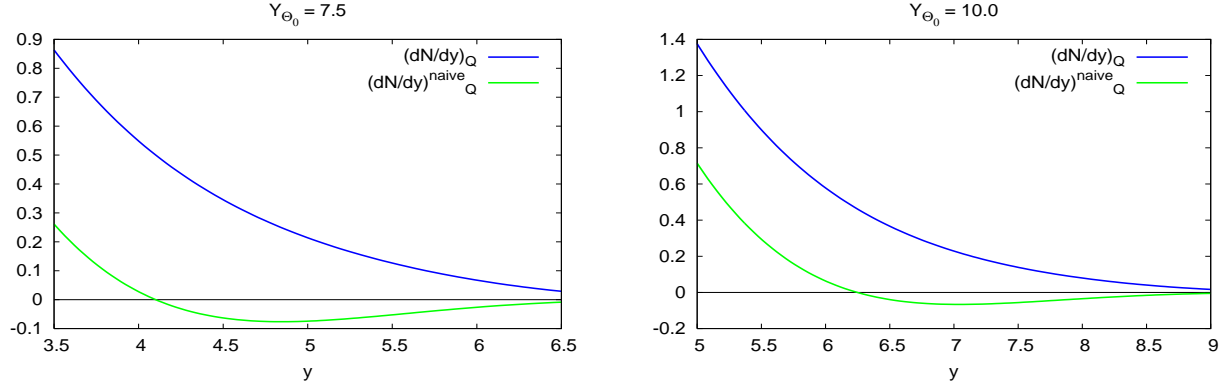


Fig. 10: enlargements of Fig. 9 at large k_\perp

5.3 Role of the lower limit of integration ℓ_{min}

To get an estimate of the sensitivity of the calculation of $\frac{dN}{d\ln k_\perp}$ to the lower bound of integration in (42), we plot in Fig. 11 below the two results obtained at $Y_{\Theta_0} = 7.5$ for $\ell_{min} = 2$ and $\ell_{min} = 0$, for a gluon jet (left) and a quark jet (right).

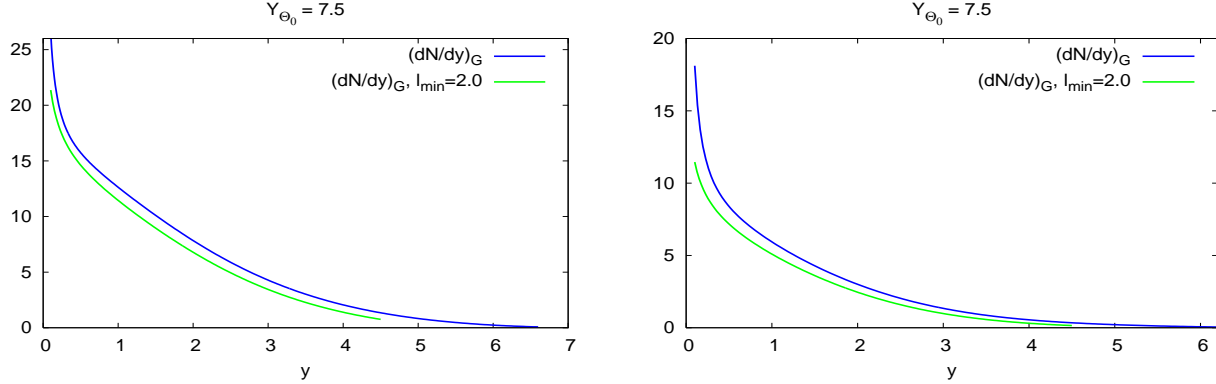


Fig. 11: $\frac{dN}{d\ln k_\perp}$ with $\ell_{min} = 2$ and $\ell_{min} = 0$ for gluon (left) and quark (right) jet.

The shapes of the corresponding distributions are identical; they only differ by a vertical shift which is small in the perturbative region $y \geq 1$ (restricting the domain of integration – increasing ℓ_{min} – results as expected in a decrease of $\frac{dN}{d\ln k_\perp}$). This shows that, though our calculation is only valid at small x_1 , the sensitivity of the final result to this parameter is small.

5.4 Discussion

MLLA corrections are seen on Fig. 8 and Fig. 10 to cure the problems of positivity which occur in the naive approach.

The range of ℓ_1 integration in the definition (42) of $\frac{dN}{d\ln k_\perp}$ should be such that, at least, its upper bound corresponds to x_1 small enough; we have seen in the discussion of MLLA corrections to the color current in subsection 4.1 that one should reasonably consider $\ell_1 \geq 2.5$; at fixed Y_{Θ_0} this yields the upper bound $y_1 \leq Y_{\Theta_0} - 2.5$, that is, at LHC $y_1 \leq 5$.

On the other side, the perturbative regime we suppose to start at $y_1 \geq 1$. These mark the limits of the interval where our calculation can be trusted $1 \leq y_1 \leq 5$ at LHC. For $y_1 < 1$ non-perturbative corrections will dominate, and for $y_1 > Y_{\Theta_0} - \ell_1^{min} \approx Y_{\Theta_0} - 2.5$, the integration defining $\frac{dN}{d\ln k_\perp}$ ranges over values of x_1 which lie outside our small x approximation and for which the MLLA corrections become accordingly out of control.

On the curves of Figs. 7 and 9 at $Y_{\Theta_0} = 10$, the small y region exhibits a bump which comes from the competition between two phenomena: the divergence of $\alpha_s(k_\perp^2)$ when $k_\perp \rightarrow Q_0$ and coherence effects which deplete multiple production at very small momentum. The separation of these two effects is still more visible at $Y_{\Theta_0} = 15$, which is studied in appendix E.3, where a comparison with DLA calculations is performed. At smaller Y_{Θ_0} , the divergence of α_s wins over coherence effects and the bump disappears. The curves corresponding to the LEP and Tevatron working conditions are given in appendix D.

5.4.1 Mixed quark and gluon jets

In many experiments, the nature of the jet (quark or gluon) is not determined, and one simply detects outgoing hadrons, which can originate from either type; one then introduces a “mixing” parameter ω ,

which is to be determined experimentally, such that, for example if one deals with the inclusive k_\perp distribution

$$\left(\frac{dN}{d \ln k_\perp} \right)_{mixed} = \omega \left(\frac{dN}{d \ln k_\perp} \right)_g + (1 - \omega) \left(\frac{dN}{d \ln k_\perp} \right)_q. \quad (43)$$

It is in this framework that forthcoming data from the LHC will be compared with our theoretical predictions; since outgoing charged hadrons are detected, one introduces the phenomenological parameter \mathcal{K}^{ch} [1][7] normalizing partonic distributions to the ones of charged hadrons

$$\left(\frac{dN}{d \ln k_\perp} \right)^{ch} = \mathcal{K}^{ch} \left(\frac{dN}{d \ln k_\perp} \right)_{mixed}. \quad (44)$$

6 CONCLUSION

After deducing a general formula, valid for all x , for the double differential 2-particle inclusive cross section for jet production in a hard collision process, the exact solutions of the MLLA evolution equations [8] have been used to perform a small x calculation of the double differential 1-particle inclusive distributions and of the inclusive k_\perp distributions for quark and gluon jets.

Sizable differences with the naive approach in which one forgets the jet evolution between its opening angle Θ_0 and the emission angle Θ have been found; their role is emphasized to recover, in particular, the positivity of the distributions.

MLLA corrections increase with x and decrease when the transverse momentum k_\perp of the outgoing hadrons gets larger; that they stay “within control” requires in practice that the small x region should not be extended beyond $\ell < 2.5$; it is remarkable that similar bounds arise in the study of 2-particle correlations [9]. At fixed Y_{Θ_0} , the lower bound for ℓ translates into an upper bound for y ; this fixes in particular the upper limit of confidence for our calculation of $\frac{dN}{d \ln k_\perp}$; above this threshold, though k_\perp is larger (more “perturbative”), the small x approximation is no longer valid.

The “divergent” behavior of the MLLA distributions for $y \rightarrow 0$ forbids extending the confidence domain of MLLA lower than $y \geq 1$, keeping away from the singularity of $\alpha_s(k_\perp^2)$ when $k_\perp \rightarrow \Lambda_{QCD}$.

The two (competing) effects of coherence (damping of multiple production at small momentum) and divergence of $\alpha_s(k_\perp^2)$ at small k_\perp for the inclusive k_\perp distribution have been exhibited.

MLLA and DLA calculations have been compared; in “modified” MLLA calculations, we have furthermore factored out the α_s dependence to ease the comparison with DLA.

While the goal of this work is a comparison of our theoretical predictions with forthcoming data from LHC and Tevatron, we have also given results for LEP. LHC energies will provide a larger trustable domain of comparison with theoretical predictions at small x .

Further developments of this work aim at getting rid of the limit $Q_0 \approx \Lambda_{QCD}$ and extending the calculations to a larger range of values of x ; then, because of the lack of analytical expressions, the general formulæ (19) and (20) should be numerically investigated, which will also provide a deeper insight into the connection between DGLAP and MLLA evolution equations [16].

Acknowledgments: *It is a pleasure to thank M. Cacciari, Yu.L. Dokshitzer and G.P. Salam for many stimulating discussions, and for expert help in numerical calculations. R. P-R. wants to specially thank Y.L. Dokshitzer for his guidance and encouragements.*

APPENDIX

A EXACT SOLUTION OF THE MLLA EVOLUTION EQUATION FOR THE FRAGMENTATION FUNCTIONS; THE SPECTRUM AND ITS DERIVATIVES

A.1 MLLA evolution equation for a gluon jet

Because of (32), we will only write the evolution equations for gluonic fragmentation functions D_g^b .

The partonic structure functions D_a^b satisfy an evolution equation which is best written when expressed in terms of the variables ℓ and y and the functions \tilde{D}_a^b defined by [1] (see also (21) (23)):

$$x_b D_a^b(x_b, k_a, q) = \tilde{D}_a^b(\ell_b, y_b). \quad (45)$$

The parton content \tilde{D}_g of a gluon is shown in [8] to satisfy the evolution equation (Y and y are linked by (6))

$$\tilde{D}_g(\ell, y) = \delta(\ell) + \int_0^y dy' \int_0^\ell d\ell' \gamma_0^2(\ell' + y') [1 - a\delta(\ell' - \ell)] \tilde{D}_g(\ell', y'), \quad (46)$$

where the anomalous dimension $\gamma_0(y)$ is given by (λ is defined in (39))

$$\gamma_0^2(y) = 4N_c \frac{\alpha_s(k_\perp^2)}{2\pi} \approx \frac{1}{\beta(y + \lambda)}. \quad (47)$$

(see the beginning of section 2 for β , T_R , C_F , α_s , N_c) and

$$a = \frac{1}{4N_c} \left[\frac{11}{3}N_c + \frac{4}{3}T_R \left(1 - \frac{2C_F}{N_c} \right) \right]; \quad C_F = 4/3 \text{ for } SU(3)_c. \quad (48)$$

The (single logarithmic) subtraction term proportional to a in (46) accounts for *gluon \rightarrow quark* transitions in parton cascades as well as for energy conservation – the so-called “hard corrections” to parton cascading –.

No superscript has been written in the structure functions D_g because the same equation is valid indifferently for D_g^g and D_g^q (see section 4). One considers that the same evolution equations govern the (inclusive) hadronic distributions D_g^h (Local Hadron Parton Duality).

A.2 Exact solution of the MLLA evolution equation for particle spectra

The exact solution of the evolution equation (46), which includes constraints of energy conservation and the running of α_s , is demonstrated in [8] to be given by the following Mellin’s representation

$$\begin{aligned} \tilde{D}_g(\ell, y, \lambda) &= (\ell + y + \lambda) \int \frac{d\omega}{2\pi i} \int \frac{d\nu}{2\pi i} e^{\omega\ell + \nu y} \\ &\quad \int_0^\infty \frac{ds}{\nu + s} \left(\frac{\omega(\nu + s)}{(\omega + s)\nu} \right)^{1/(\beta(\omega - \nu))} \left(\frac{\nu}{\nu + s} \right)^{a/\beta} e^{-\lambda s}. \end{aligned} \quad (49)$$

From (49) and taking the high energy limit $\ell + y \equiv Y \gg \lambda$ ⁹ one gets [1][7] the explicit formula

$$\tilde{D}_g(\ell, y) = \frac{\ell + y}{\beta B(B+1)} \int \frac{d\omega}{2\pi i} e^{-\omega y} \Phi(A+1, B+2, \omega(\ell+y)), \quad (50)$$

where Φ is the confluent hypergeometric function the integral representation of which reads [17] [18]

$$\Phi(A+1, B+2, \omega Y) = \Gamma(B+2) (\omega Y)^{-B-1} \int \frac{dt}{(2\pi i)} \frac{t^{-B}}{t(t-1)} \left(\frac{t}{t-1} \right)^A e^{\omega Y t};$$

with $A = \frac{1}{\beta\omega}$, $B = \frac{a}{\beta}$, $\Gamma(n) = \int_0^\infty d\chi \chi^{n-1} e^{-\chi}$. (51)

Exchanging the t and ω integrations of (50) (51) and going from t to the new variable $\alpha = \frac{1}{2} \ln \frac{t}{t-1}$, (50) becomes

$$\tilde{D}_g(\ell, y) = 2 \frac{\Gamma(B)}{\beta} \Re \left(\int_0^{\frac{\pi}{2}} \frac{d\tau}{\pi} e^{-B\alpha} \mathcal{F}_B(\tau, y, \ell) \right), \quad (52)$$

where the integration is performed with respect to τ defined by $\alpha = \frac{1}{2} \ln \frac{y}{\ell} + i\tau$,

$$\mathcal{F}_B(\tau, y, \ell) = \left[\frac{\cosh \alpha - \frac{y-\ell}{y+\ell} \sinh \alpha}{\frac{\ell+y}{\beta} \frac{\alpha}{\sinh \alpha}} \right]^{B/2} I_B(2\sqrt{Z(\tau, y, \ell)}),$$

$$Z(\tau, y, \ell) = \frac{\ell+y}{\beta} \frac{\alpha}{\sinh \alpha} \left(\cosh \alpha - \frac{y-\ell}{y+\ell} \sinh \alpha \right); \quad (53)$$

I_B is the modified Bessel function of the first kind.

A.3 The spectrum

On Fig. 12 below, we represent, on the left, the spectrum as a function of the transverse momentum (via y) for fixed ℓ and, on the right, as a function of the energy (via ℓ) for fixed transverse momentum.

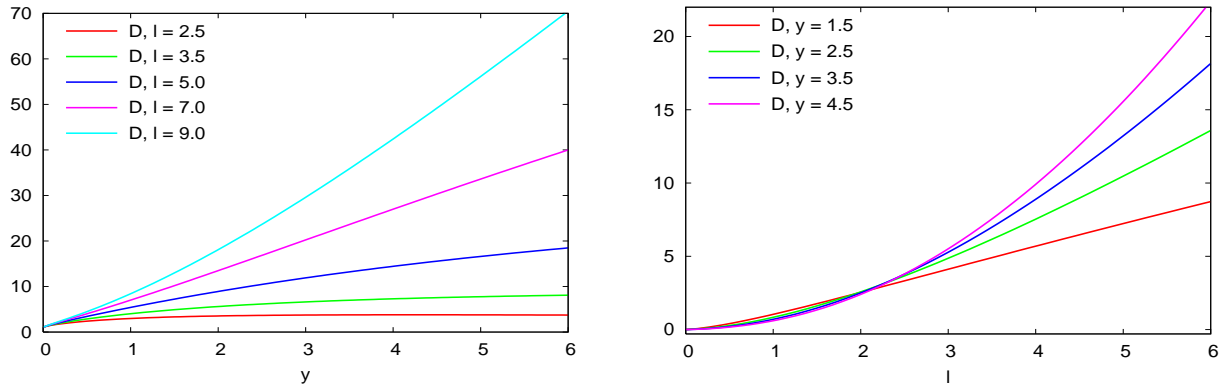


Fig. 12: spectrum $\tilde{D}(\ell, y)$ of emitted partons
as functions of transverse momentum (left) and energy (right)

⁹ $Y \gg \lambda \Leftrightarrow E\Theta \gg Q_0^2/\Lambda_{QCD}$ is not strictly equivalent to $Q_0 \rightarrow \Lambda_{QCD}$ (limiting spectrum).

Fig. 13 shows enlargements of Fig. 12 for small values of y and ℓ respectively; they ease the understanding of the curves for the derivatives of the spectrum presented in subsection A.4.

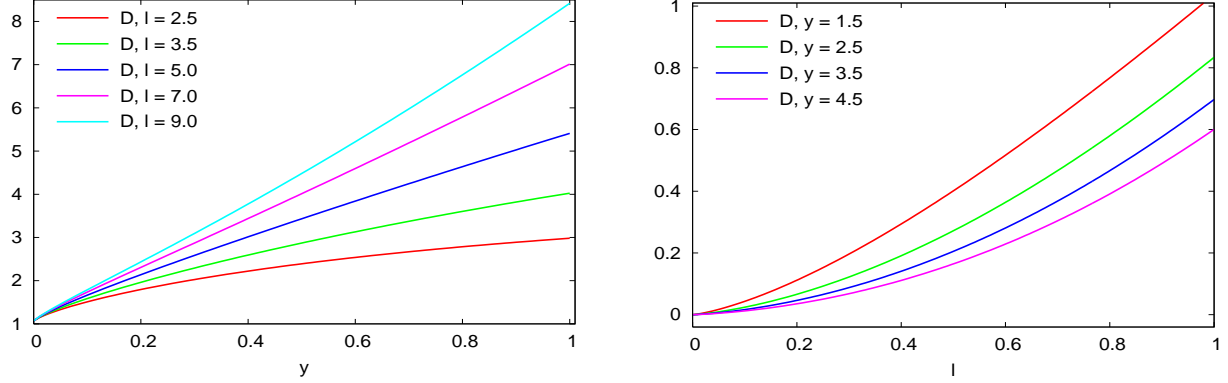


Fig. 13: spectrum $\tilde{D}(\ell, y)$ of emitted partons as functions of transverse momentum (left) and energy (right): enlargement of Fig. 12

A comparison between MLLA and DLA calculations of the spectrum is done in appendix E.1.

A.4 Derivatives of the spectrum

We evaluate below the derivatives of the spectrum w.r.t. $\ln k_\perp$ and $\ln(1/x)$.

We make use of the following property for the confluent hypergeometric functions Φ [18]:

$$\frac{d}{d\ell} \Phi(A+1, B+2, \omega(\ell+y)) \equiv \frac{d}{dy} \Phi(A+1, B+2, \omega(\ell+y)) = \omega \frac{A+1}{B+2} \Phi(A+2, B+3, \omega(\ell+y)). \quad (54)$$

- We first determine the derivative w.r.t. $\ell \equiv \ln(1/x)$. Differentiating (50) w.r.t. ℓ , and expanding (54), one gets ¹⁰ [8]

$$\frac{d}{d\ell} \tilde{D}_g(\ell, y) = 2 \frac{\Gamma(B)}{\beta} \int_0^{\frac{\pi}{2}} \frac{d\tau}{\pi} e^{-B\alpha} \left[\frac{1}{\ell+y} (1 + 2e^\alpha \sinh \alpha) \mathcal{F}_B + \frac{1}{\beta} e^\alpha \mathcal{F}_{B+1} \right]; \quad (55)$$

- Differentiating w.r.t. $y \equiv \ln \frac{k_\perp}{Q_0}$ yields

$$\frac{d}{dy} \tilde{D}_g(\ell, y) = 2 \frac{\Gamma(B)}{\beta} \int_0^{\frac{\pi}{2}} \frac{d\tau}{\pi} e^{-B\alpha} \left[\frac{1}{\ell+y} (1 + 2e^\alpha \sinh \alpha) \mathcal{F}_B + \frac{1}{\beta} e^\alpha \mathcal{F}_{B+1} - \frac{2 \sinh \alpha}{\ell+y} \mathcal{F}_{B-1} \right]. \quad (56)$$

In Fig. 14, Fig. 15, Fig. 16 and Fig. 17 below, we draw the curves for:

- * $\frac{d\tilde{D}_g(\ell, y)}{dy}$ as a function of y , for different values of ℓ fixed;
- * $\frac{d\tilde{D}_g(\ell, y)}{d\ell}$ as a function of ℓ , for different values of y fixed;

¹⁰(55) and (56) have also been checked by numerically differentiating (52).

- * $\frac{d\tilde{D}_g(\ell, y)}{d\ell}$ as a function of ℓ for different values of y fixed;
- * $\frac{d\tilde{D}_g(\ell, y)}{dy}$ as a function of y for different values of ℓ fixed.

In each case the right figure is an enlargement, close to the origin of axes, of the left figure.

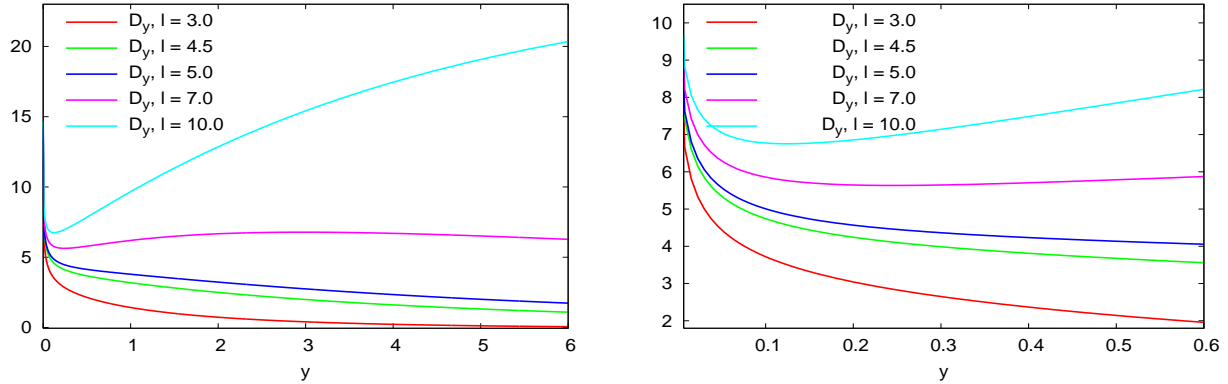


Fig. 14: $\frac{d\tilde{D}_g(\ell, y)}{dy}$ as a function of y for different values of ℓ

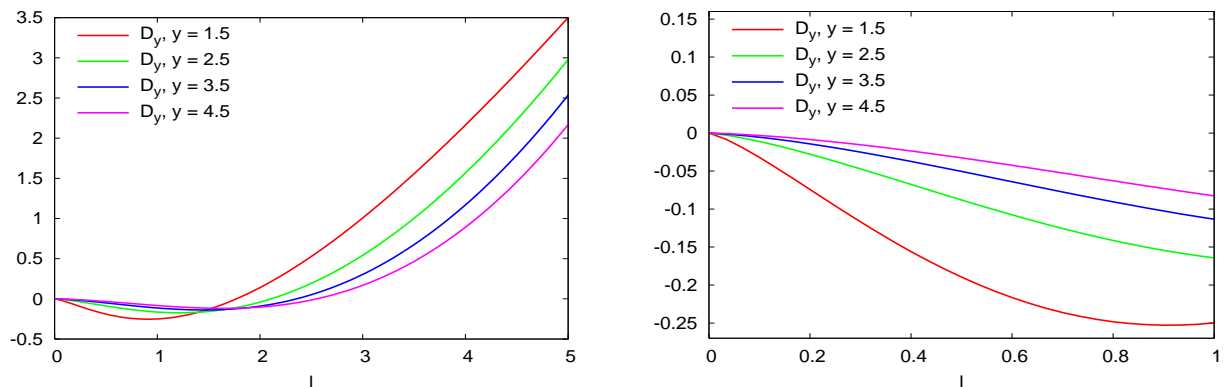


Fig. 15: $\frac{d\tilde{D}_g(\ell, y)}{dy}$ as a function of ℓ for different values of y

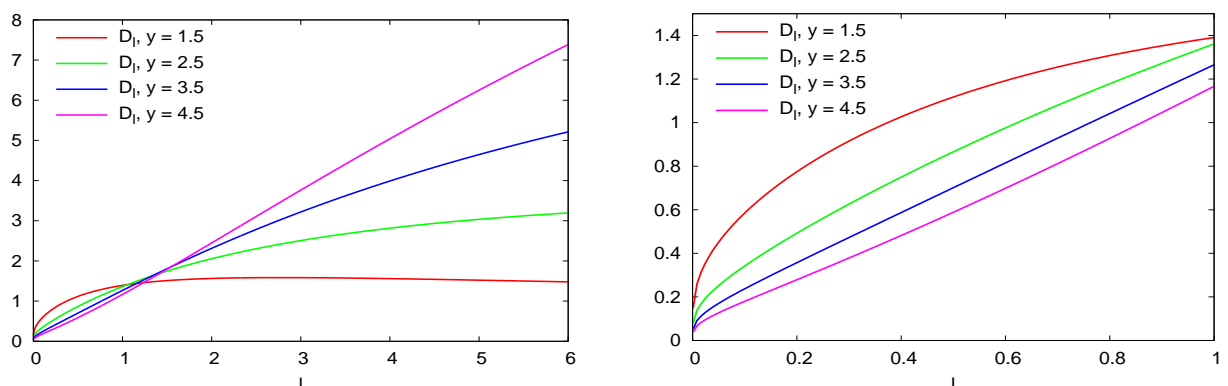


Fig. 16: $\frac{d\tilde{D}_g(\ell, y)}{dl}$ as a function of ℓ for different values of y

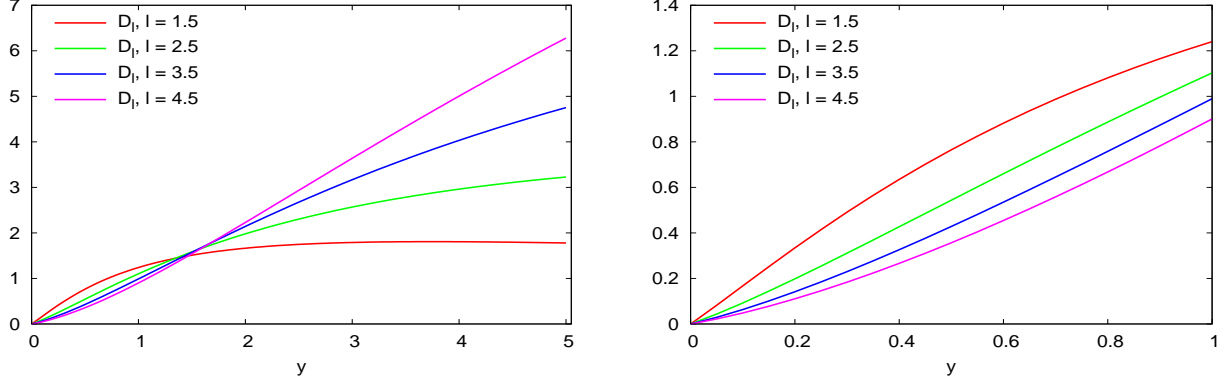


Fig. 17: $\frac{d\tilde{D}_g(\ell, y)}{d\ell}$ as a function of y for different values of ℓ

That $\frac{d\tilde{D}_g(\ell, y)}{dy}$ goes to infinity when $y \rightarrow 0$ is in agreement with the analytic behavior in $\ln(\ell/y)$ of this derivative.

B LEADING CONTRIBUTIONS TO $x_1 F_{A_0}^{h_1}(x_1, \Theta, E, \Theta_0)$ AT SMALL x_1

Using (32), the leading terms of $x_1 F_{A_0}^{h_1}(x_1, \Theta, E, \Theta_0)$ (26) calculated at small x_1 read

$$\begin{aligned} x_1 F_g^{h_1}(x_1, \Theta, E, \Theta_0)^0 &\approx \tilde{D}_g(\ell_1, y_1) \left(\langle u \rangle_g^g + \frac{C_F}{N_c} \langle u \rangle_g^q \right) = \frac{\langle C \rangle_g^0}{N_c} \tilde{D}_g(\ell_1, y_1), \\ x_1 F_q^{h_1}(x_1, \Theta, E, \Theta_0)^0 &\approx \tilde{D}_g(\ell_1, y_1) \left(\langle u \rangle_q^g + \frac{C_F}{N_c} \langle u \rangle_q^q \right) = \frac{\langle C \rangle_q^0}{N_c} \tilde{D}_g(\ell_1, y_1). \end{aligned} \quad (57)$$

The leading $\langle C \rangle_g^0$ and $\langle C \rangle_q^0$ in (34) for a quark and a gluon jet are given respectively by (see [1], chapt. 9¹¹)

$$\begin{aligned} \langle C \rangle_q^0 &= \langle C \rangle_\infty - c_1 (N_c - C_F) \left(\frac{\ln(E\Theta/\Lambda_{QCD})}{\ln(E\Theta_0/\Lambda_{QCD})} \right)^{(c_3/4N_c\beta)} \\ &= \langle C \rangle_\infty - c_1 (N_c - C_F) \left(\frac{Y_\Theta + \lambda}{Y_{\Theta_0} + \lambda} \right)^{(c_3/4N_c\beta)}, \end{aligned} \quad (58)$$

$$\begin{aligned} \langle C \rangle_g^0 &= \langle C \rangle_\infty + c_2 (N_c - C_F) \left(\frac{\ln(E\Theta/\Lambda_{QCD})}{\ln(E\Theta_0/\Lambda_{QCD})} \right)^{(c_3/4N_c\beta)} \\ &= \langle C \rangle_\infty + c_2 (N_c - C_F) \left(\frac{Y_\Theta + \lambda}{Y_{\Theta_0} + \lambda} \right)^{(c_3/4N_c\beta)}, \end{aligned} \quad (59)$$

¹¹The coefficient β , omitted in the exponents of eqs. (9.12a), (9.12b), (9.12c) of [1] has been restored here. The factor $4N_c$ is due to our normalization (see the beginning of section 2).

with

$$\begin{aligned} < C >_\infty &= c_1 N_c + c_2 C_F, \\ c_1 = \frac{8}{3} \frac{C_F}{c_3}, \quad c_2 &= 1 - c_1 = \frac{2}{3} \frac{n_f}{c_3}, \quad c_3 = \frac{8}{3} C_F + \frac{2}{3} n_f; \end{aligned} \quad (60)$$

in the r.h.s of (58) (59) we have used the definitions (6) (7). $< C >_\infty$ corresponds to the limit $E \rightarrow \infty, \Theta \rightarrow 0$.

In practice, we take in this work

$$Q_0 \approx \Lambda_{QCD} \Leftrightarrow \lambda \approx 0, \quad (61)$$

which ensures in particular the consistency with the analytical calculation of the MLLA spectrum (appendix A), which can only be explicitly achieved in this limit.

C CALCULATION OF $\delta < C >_g$ AND $\delta < C >_q$ OF SECTION 4

C.1 Explicit expressions for $< u >_{A_0}^A$ and $\delta < u >_{A_0}^A$ defined in (28)

The expressions (28) for $< u >_{A_0}^A$ and $\delta < u >_{A_0}^A$ are conveniently obtained from the Mellin-transformed DGLAP fragmentation functions [1]

$$\mathcal{D}(j, \xi) = \int_0^1 du u^{j-1} D(u, \xi), \quad (62)$$

which, if one deals with $D_A^B(u, r^2, s^2)$, depends in reality on the difference $\xi(r^2) - \xi(s^2)$:

$$\xi(Q^2) = \int_{\mu^2}^{Q^2} \frac{dk^2}{k^2} \frac{\alpha_s(k^2)}{4\pi}, \quad \xi(r^2) - \xi(s^2) \approx \frac{1}{4N_c\beta} \ln \left(\frac{\ln(r^2/\Lambda_{QCD}^2)}{\ln(s^2/\Lambda_{QCD}^2)} \right). \quad (63)$$

One has accordingly

$$< u >_{A_0}^A = \mathcal{D}_{A_0}^A(2, \xi(E\Theta_0) - \xi(E\Theta)), \quad \delta < u >_{A_0}^A = \frac{d}{dj} \mathcal{D}_{A_0}^A(j, \xi(E\Theta_0) - \xi(E\Theta)) \Big|_{j=2}. \quad (64)$$

The DGLAP functions $\mathcal{D}(j, \xi)$ are expressed [1] in terms of the anomalous dimensions $\nu_F(j)$, $\nu_G(j)$ and $\nu_\pm(j)$, the j dependence of which is in particular known.

For the sake of completeness, we give below the expressions for the $< u >$'s and $\delta < u >$'s.

$$\begin{aligned} < u >_g^q &= \frac{9}{25} \left(\left(\frac{Y_{\Theta_0} + \lambda}{Y_\Theta + \lambda} \right)^{\frac{50}{81}} - 1 \right) \left(\frac{Y_{\Theta_0} + \lambda}{Y_\Theta + \lambda} \right)^{-\frac{50}{81}}, \\ < u >_g^g &= 1/25 \left(16 \left(\frac{Y_{\Theta_0} + \lambda}{Y_\Theta + \lambda} \right)^{\frac{50}{81}} + 9 \right) \left(\frac{Y_{\Theta_0} + \lambda}{Y_\Theta + \lambda} \right)^{-\frac{50}{81}}, \\ < u >_q^g &= \frac{16}{25} \left(\left(\frac{Y_{\Theta_0} + \lambda}{Y_\Theta + \lambda} \right)^{\frac{50}{81}} - 1 \right) \left(\frac{Y_{\Theta_0} + \lambda}{Y_\Theta + \lambda} \right)^{-\frac{50}{81}}, \end{aligned}$$

$$\langle u \rangle_q^{sea} = -1/25 \left(-9 \left(\frac{Y_{\Theta_0} + \lambda}{Y_{\Theta} + \lambda} \right)^{\frac{50}{81}} - 16 + 25 \left(\frac{Y_{\Theta_0} + \lambda}{Y_{\Theta} + \lambda} \right)^{2/9} \right) \left(\frac{Y_{\Theta_0} + \lambda}{Y_{\Theta} + \lambda} \right)^{-\frac{50}{81}},$$

$$\langle u \rangle^{val} = \left(\frac{Y_{\Theta_0} + \lambda}{Y_{\Theta} + \lambda} \right)^{-\frac{32}{81}},$$

$$\langle u \rangle_q^{sea} + \langle u \rangle^{val} = 1/25 \left(9 \left(\frac{Y_{\Theta_0} + \lambda}{Y_{\Theta} + \lambda} \right)^{\frac{50}{81}} + 16 \right) \left(\frac{Y_{\Theta_0} + \lambda}{Y_{\Theta} + \lambda} \right)^{-\frac{50}{81}};$$

$$\begin{aligned} \delta \langle u \rangle_g^q &= -\frac{1}{337500} \left(-43011 \left(\frac{Y_{\Theta_0} + \lambda}{Y_{\Theta} + \lambda} \right)^{\frac{50}{81}} + 43011 - 6804 \pi^2 \left(\frac{Y_{\Theta_0} + \lambda}{Y_{\Theta} + \lambda} \right)^{\frac{50}{81}} \right. \\ &\quad + 6804 \pi^2 - 48600 \ln \left(\frac{Y_{\Theta_0} + \lambda}{Y_{\Theta} + \lambda} \right) \left(\frac{Y_{\Theta_0} + \lambda}{Y_{\Theta} + \lambda} \right)^{\frac{50}{81}} \\ &\quad + 21600 \ln \left(\frac{Y_{\Theta_0} + \lambda}{Y_{\Theta} + \lambda} \right) \left(\frac{Y_{\Theta_0} + \lambda}{Y_{\Theta} + \lambda} \right)^{\frac{50}{81}} \pi^2 + 109525 \ln \left(\frac{Y_{\Theta_0} + \lambda}{Y_{\Theta} + \lambda} \right) \\ &\quad \left. - 17400 \ln \left(\frac{Y_{\Theta_0} + \lambda}{Y_{\Theta} + \lambda} \right) \pi^2 \right) \left(\frac{Y_{\Theta_0} + \lambda}{Y_{\Theta} + \lambda} \right)^{-\frac{50}{81}}, \end{aligned}$$

$$\begin{aligned} \delta \langle u \rangle_g^g &= -\frac{1}{337500} \left(-11664 \left(\frac{Y_{\Theta_0} + \lambda}{Y_{\Theta} + \lambda} \right)^{\frac{50}{81}} + 31104 \pi^2 \left(\frac{Y_{\Theta_0} + \lambda}{Y_{\Theta} + \lambda} \right)^{\frac{50}{81}} \right. \\ &\quad - 86400 \ln \left(\frac{Y_{\Theta_0} + \lambda}{Y_{\Theta} + \lambda} \right) \left(\frac{Y_{\Theta_0} + \lambda}{Y_{\Theta} + \lambda} \right)^{\frac{50}{81}} \\ &\quad + 38400 \ln \left(\frac{Y_{\Theta_0} + \lambda}{Y_{\Theta} + \lambda} \right) \left(\frac{Y_{\Theta_0} + \lambda}{Y_{\Theta} + \lambda} \right)^{\frac{50}{81}} \pi^2 \\ &\quad + 11664 - 31104 \pi^2 - 109525 \ln \left(\frac{Y_{\Theta_0} + \lambda}{Y_{\Theta} + \lambda} \right) \\ &\quad \left. + 17400 \ln \left(\frac{Y_{\Theta_0} + \lambda}{Y_{\Theta} + \lambda} \right) \pi^2 \right) \left(\frac{Y_{\Theta_0} + \lambda}{Y_{\Theta} + \lambda} \right)^{-\frac{50}{81}}, \end{aligned}$$

$$\begin{aligned} \delta \langle u \rangle_q^g &= -\frac{4}{759375} \left(48114 \left(\frac{Y_{\Theta_0} + \lambda}{Y_{\Theta} + \lambda} \right)^{\frac{50}{81}} - 48114 - 6804 \pi^2 \left(\frac{Y_{\Theta_0} + \lambda}{Y_{\Theta} + \lambda} \right)^{\frac{50}{81}} \right. \\ &\quad + 6804 \pi^2 - 48600 \ln \left(\frac{Y_{\Theta_0} + \lambda}{Y_{\Theta} + \lambda} \right) \left(\frac{Y_{\Theta_0} + \lambda}{Y_{\Theta} + \lambda} \right)^{\frac{50}{81}} \\ &\quad + 21600 \ln \left(\frac{Y_{\Theta_0} + \lambda}{Y_{\Theta} + \lambda} \right) \left(\frac{Y_{\Theta_0} + \lambda}{Y_{\Theta} + \lambda} \right)^{\frac{50}{81}} \pi^2 + 109525 \ln \left(\frac{Y_{\Theta_0} + \lambda}{Y_{\Theta} + \lambda} \right) \\ &\quad \left. - 17400 \ln \left(\frac{Y_{\Theta_0} + \lambda}{Y_{\Theta} + \lambda} \right) \pi^2 \right) \left(\frac{Y_{\Theta_0} + \lambda}{Y_{\Theta} + \lambda} \right)^{-\frac{50}{81}}, \end{aligned}$$

$$\delta \langle u \rangle_q^{sea} = \frac{2}{759375} \left(-13122 \left(\frac{Y_{\Theta_0} + \lambda}{Y_{\Theta} + \lambda} \right)^{\frac{50}{81}} + 34992 \pi^2 \left(\frac{Y_{\Theta_0} + \lambda}{Y_{\Theta} + \lambda} \right)^{\frac{50}{81}} \right)$$

$$\begin{aligned}
& + 54675 \ln \left(\frac{Y_{\Theta_0} + \lambda}{Y_{\Theta} + \lambda} \right) \left(\frac{Y_{\Theta_0} + \lambda}{Y_{\Theta} + \lambda} \right)^{\frac{50}{81}} \\
& - 24300 \ln \left(\frac{Y_{\Theta_0} + \lambda}{Y_{\Theta} + \lambda} \right) \left(\frac{Y_{\Theta_0} + \lambda}{Y_{\Theta} + \lambda} \right)^{\frac{50}{81}} \pi^2 \\
& + 13122 - 34992 \pi^2 + 219050 \ln \left(\frac{Y_{\Theta_0} + \lambda}{Y_{\Theta} + \lambda} \right) - 34800 \ln \left(\frac{Y_{\Theta_0} + \lambda}{Y_{\Theta} + \lambda} \right) \pi^2 \\
& - 265625 \ln \left(\frac{Y_{\Theta_0} + \lambda}{Y_{\Theta} + \lambda} \right) \left(\frac{Y_{\Theta_0} + \lambda}{Y_{\Theta} + \lambda} \right)^{\frac{2}{9}} \\
& + 37500 \ln \left(\frac{Y_{\Theta_0} + \lambda}{Y_{\Theta} + \lambda} \right) \left(\frac{Y_{\Theta_0} + \lambda}{Y_{\Theta} + \lambda} \right)^{\frac{2}{9}} \pi^2 \Big) \left(\frac{Y_{\Theta_0} + \lambda}{Y_{\Theta} + \lambda} \right)^{-\frac{50}{81}}, \\
\delta < u >^{val} &= -\frac{2}{243} (-85 + 12 \pi^2) \ln \left(\frac{Y_{\Theta_0} + \lambda}{Y_{\Theta} + \lambda} \right) \left(\frac{Y_{\Theta_0} + \lambda}{Y_{\Theta} + \lambda} \right)^{-\frac{32}{81}}, \\
\delta < u >^{val} + \delta < u >_q^{sea} &= -\frac{2}{759375} \left(13122 \left(\frac{Y_{\Theta_0} + \lambda}{Y_{\Theta} + \lambda} \right)^{\frac{50}{81}} - 34992 \pi^2 \left(\frac{Y_{\Theta_0} + \lambda}{Y_{\Theta} + \lambda} \right)^{\frac{50}{81}} \right. \\
&\quad - 54675 \ln \left(\frac{Y_{\Theta_0} + \lambda}{Y_{\Theta} + \lambda} \right) \left(\frac{Y_{\Theta_0} + \lambda}{Y_{\Theta} + \lambda} \right)^{\frac{50}{81}} \\
&\quad + 24300 \ln \left(\frac{Y_{\Theta_0} + \lambda}{Y_{\Theta} + \lambda} \right) \left(\frac{Y_{\Theta_0} + \lambda}{Y_{\Theta} + \lambda} \right)^{\frac{50}{81}} \pi^2 - 13122 + 34992 \pi^2 \\
&\quad \left. - 219050 \ln \left(\frac{Y_{\Theta_0} + \lambda}{Y_{\Theta} + \lambda} \right) + 34800 \ln \left(\frac{Y_{\Theta_0} + \lambda}{Y_{\Theta} + \lambda} \right) \pi^2 \right) \left(\frac{Y_{\Theta_0} + \lambda}{Y_{\Theta} + \lambda} \right)^{-\frac{50}{81}}. \tag{65}
\end{aligned}$$

When $\Theta \rightarrow \Theta_0$, all $\delta < u >$'s vanish, ensuring that the limits $\xi(E\Theta_0) - \xi(E\Theta) \rightarrow 0$ of the $(< C >_{A_0}^0 + \delta < C >_{A_0})$'s are the same as the ones of the $< C >_{A_0}^0$'s.

C.2 $\delta < C >_q$ and $\delta < C >_g$

They are given in (35), and one uses (32) such that only ψ_{g,ℓ_1} (see (29)) appears. Their full analytical expressions for the $\delta < C >$'s are too complicated to be easily written and manipulated.

Using the formulæ of C.1, one gets the approximate results

$$\begin{aligned}
\delta < C >_q &\approx \left(1.4676 - 1.4676 \left(\frac{Y_{\Theta_0} + \lambda}{Y_{\Theta} + \lambda} \right)^{-\frac{50}{81}} - 3.2510 \ln \left(\frac{Y_{\Theta_0} + \lambda}{Y_{\Theta} + \lambda} \right) \right. \\
&\quad \left. + 0.5461 \left(\frac{Y_{\Theta_0} + \lambda}{Y_{\Theta} + \lambda} \right)^{-\frac{50}{81}} \ln \left(\frac{Y_{\Theta_0} + \lambda}{Y_{\Theta} + \lambda} \right) \right) \psi_{g,\ell_1}(\ell_1, y_1), \tag{66}
\end{aligned}$$

and

$$\delta \langle C \rangle_g \approx \left(-2.1898 + 2.1898 \left(\frac{Y_{\Theta_0} + \lambda}{Y_{\Theta} + \lambda} \right)^{-\frac{50}{81}} - 3.2510 \ln \left(\frac{Y_{\Theta_0} + \lambda}{Y_{\Theta} + \lambda} \right) - 0.3072 \left(\frac{Y_{\Theta_0} + \lambda}{Y_{\Theta} + \lambda} \right)^{-\frac{50}{81}} \ln \left(\frac{Y_{\Theta_0} + \lambda}{Y_{\Theta} + \lambda} \right) \right) \psi_{g,\ell_1}(\ell_1, y_1). \quad (67)$$

The logarithmic derivative $\psi_{g,\ell_1}(\ell_1, y_1)$ (29) of the MLLA spectrum $\tilde{D}_g(\ell_1, y_1)$ is obtained from (52) of appendix A.

D AT LEP AND TEVATRON

At LEP energy, the working conditions correspond to $Y_{\Theta_0} \approx 5.2$; they are not very different at the Tevatron where $Y_{\Theta_0} \approx 5.6$. We first present the curves for LEP, then, after the discussion concerning the size of the corrections and the domain of validity of our calculations, we give our predictions for the Tevatron.

D.1 The average color current

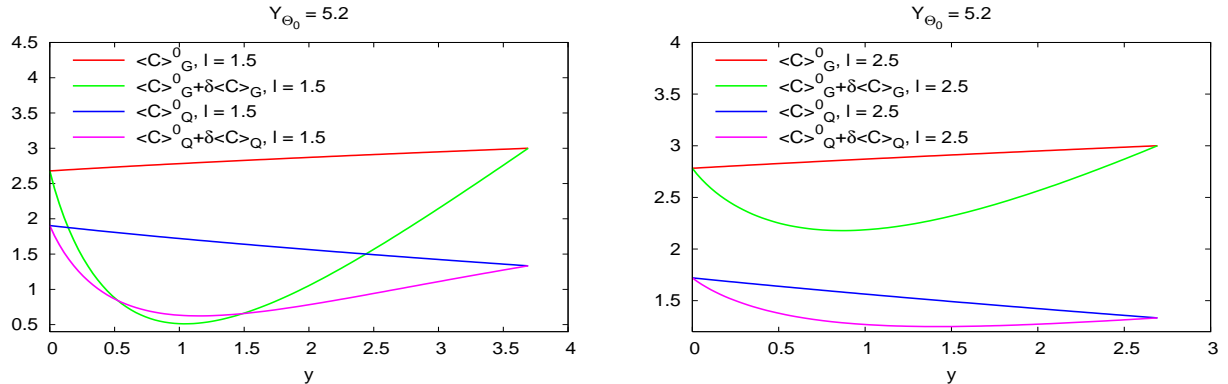


Fig. 18 $\langle C \rangle_{A_0}^0$ and $\langle C \rangle_{A_0}^0 + \delta \langle C \rangle_{A_0}$ for quark and gluon jets, as functions of y , for $Y_{\Theta_0} = 5.2$, $\ell = 1.5$ on the left and $\ell = 2.5$ on the right.

Owing to the size of the (MLLA) corrections to the $\langle C \rangle$'s and their y derivatives, we will keep to the lower bound $\ell_1 \geq 2.5$.

D.2 $\frac{d^2 N}{d\ell_1 d \ln k_\perp}$ for a gluon jet

We plot below $\frac{d^2 N}{d\ell_1 d \ln k_\perp}$ for the two values $\ell = 1.5$ and $\ell = 2.5$.

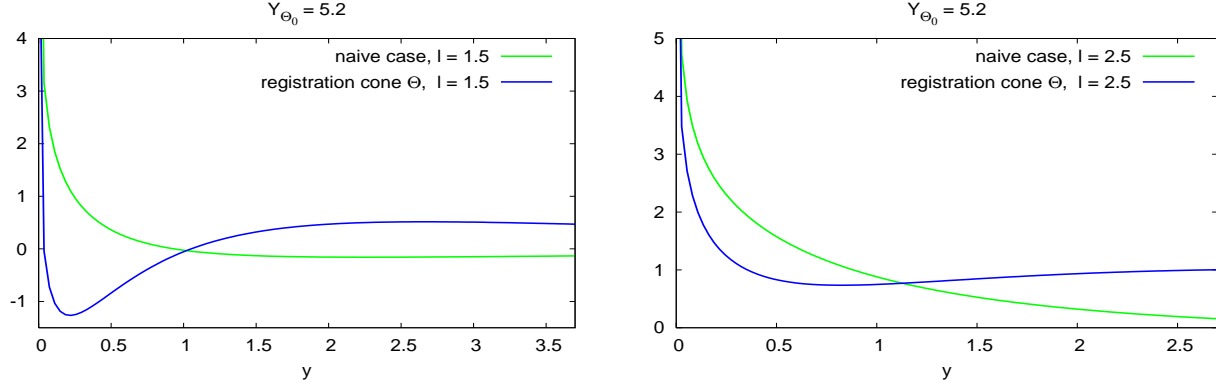


Fig. 19: $\frac{d^2N}{d\ell_1 d \ln k_\perp}$ for a gluon jet at fixed ℓ_1 , MLLA and naive approach.

The excessive size of the $\delta < C >$ corrections emphasized in subsection D.1 translates here into the loss of the positivity for $\frac{d^2N}{d\ell_1 d \ln k_\perp}$ at $\ell = 1.5$ for $y < 1$: our approximation is clearly not trustable there.

D.3 $\frac{d^2N}{d\ell_1 d \ln k_\perp}$ for a quark jet

We consider the same two values of ℓ as above.

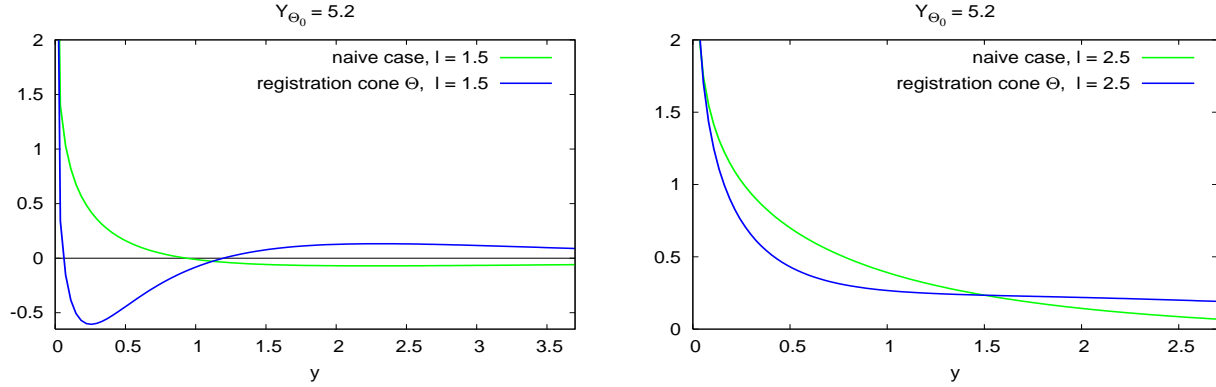


Fig. 20: $\frac{d^2N}{d\ell_1 d \ln k_\perp}$ for a quark jet at fixed ℓ_1 , MLLA and naive approach.

Like for the gluon jet, we encounter positivity problems at $\ell = 1.5$ for $y < 1.25$.

D.4 $\frac{dN}{d \ln k_\perp}$ for a gluon jet

We plot below $\frac{dN}{d \ln k_\perp}$ for a gluon jet obtained by the “naive” approach and including the jet evolution from Θ_0 to Θ ; on the right is an enlargement which shows how positivity is recovered when MLLA corrections are included.

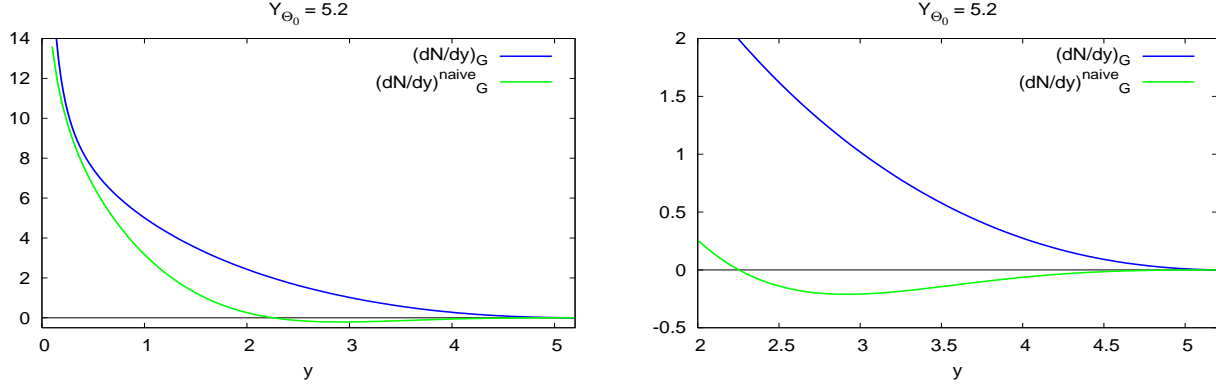


Fig. 21: $\frac{dN}{d \ln k_\perp}$ for a gluon jet, MLLA and naive approach.

D.5 $\frac{dN}{d \ln k_\perp}$ for a quark jet

We proceed like for a gluon jet. The curves below show the restoration of positivity by MLLA corrections.

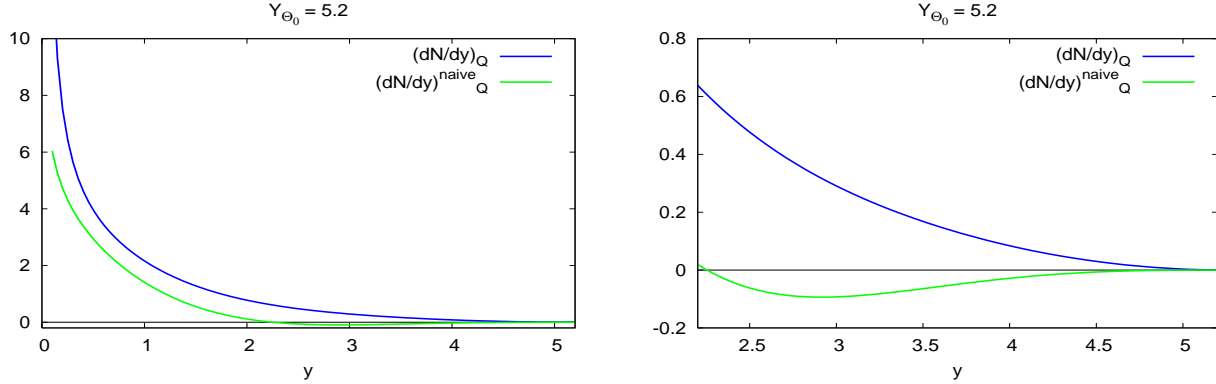


Fig. 22: $\frac{dN}{d \ln k_\perp}$ for a quark jet, MLLA and naive approach.

That the upper bound of the ℓ_1 domain of integration defining $\frac{dN}{d \ln k_\perp}$ corresponds to a large enough $\ell_1 \geq 2.5$ requires that, for LEP, y_1 should be smaller than $5.2 - 2.5 = 2.7$; combined with the necessity to stay in the perturbative regime, it yields $1 \leq y_1 \leq 2.7$.

D.6 Discussion and predictions for the Tevatron

The similar condition at Tevatron is $1 \leq y_1 \leq 5.6 - 2.5 = 3.1$; like for LEP, it does not extend to large values of k_\perp because, there, the small x approximation is no longer valid. We give below the curves that we predict in this confidence interval.

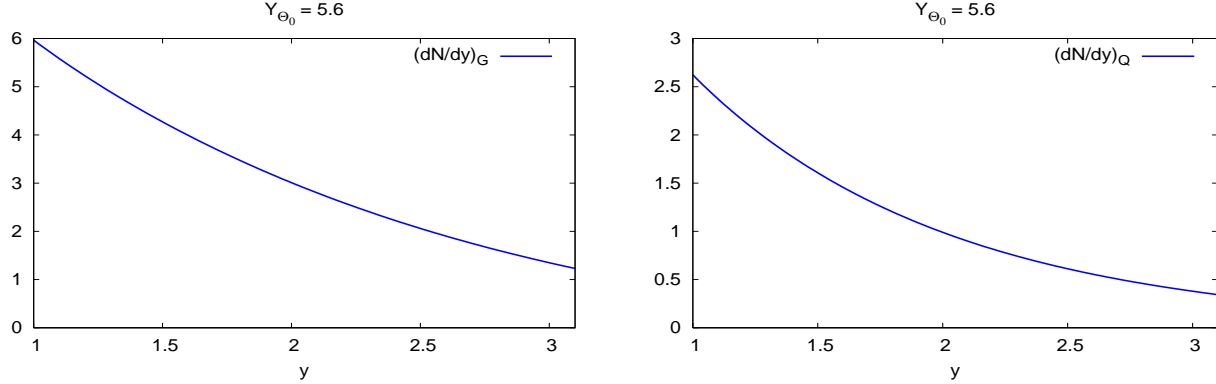


Fig. 23: $\frac{dN}{d\ln k_\perp}$ for a gluon (left) and a quark (right) jets, MLLA predictions for the Tevatron.

Since experimental results involve a mixture of gluon and quark jets, the mixing parameter ω (subsection 5.4.1) has to be introduced in the comparison with theoretical curves, together with the phenomenological factor \mathcal{K}^{ch} normalizing partonic to charge hadrons distributions.

E COMPARING DLA AND MLLA APPROXIMATIONS

DLA [14] [15] and MLLA approximations are very different [1]; in particular, the exact balance of energy (recoil effects of partons) is not accounted for in DLA.

We compare DLA and MLLA results for the two distributions of concern in this work. Studying first their difference for the spectrum itself eases the rest of the comparison.

We choose the two values $Y_{\Theta_0} = 7.5$ and $Y_{\Theta_0} = 15$. While the first corresponds to the LHC working conditions (see footnote 8), the second is purely academic since, taking for example $\Theta_0 \approx .5$ and $Q_0 \approx 250 \text{ MeV}$, it corresponds to an energy of 1635 TeV ; it is however suitable, as we shall see in subsection E.3 to disentangle the effects of coherence and the ones of the divergence of α_s at low energy in the calculation of the inclusive k_\perp distribution.

E.1 The spectrum

Fixing α_s in DLA at the largest scale of the process, the collision energy, enormously damps the corresponding spectrum (it does not take into account the growing of α_s accompanying parton cascading), which gives an unrealistic aspect to the comparison.

This is why, as far as the spectra are concerned, we shall compare their MLLA evaluation with that obtained from the latter by taking to zero the coefficient a given in (48), which also entails $B = 0$; $\mathcal{F}_0(\tau, y, \ell)$ in (53) becomes $I_0(2\sqrt{Z(\tau, y, \ell)})$. The infinite normalization that occurs in (52) because of $\Gamma(B = 0)$ we replace by a constant such that the two calculations can be easily compared. This realizes a DLA approximation (no accounting for recoil effects) “with running α_s ”.

On Fig. 24 below are plotted the spectrum $\tilde{D}_g(\ell, y \equiv Y_{\Theta_0} - \ell)$ for gluon jets in the MLLA and DLA “with running α_s ” approximations.

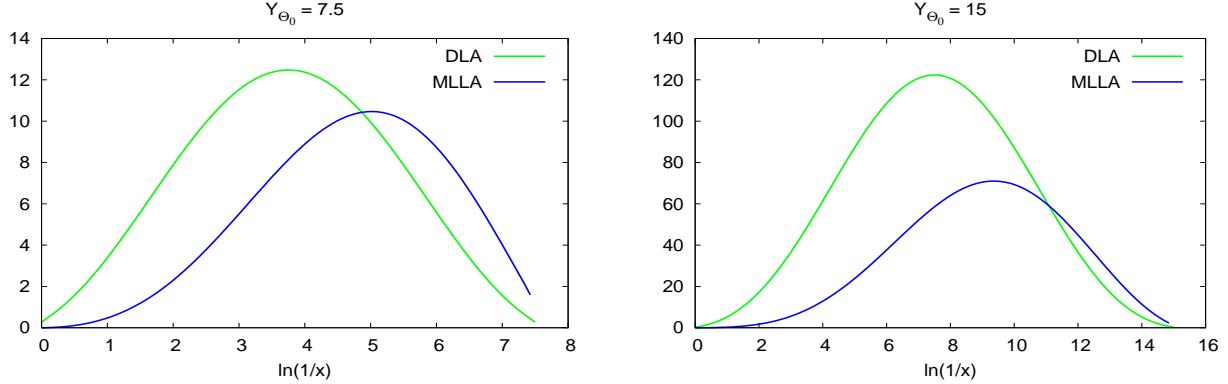


Fig. 24: the spectrum $\tilde{D}_g(\ell, Y_{\Theta_0} - \ell)$ for gluon jets; comparison between MLLA and DLA (“with running α_s ”) calculations.

The peak of the MLLA spectrum is seen, as expected, to occur at smaller values of the energy than that of DLA.

E.2 Double differential 1-particle inclusive distribution

The genuine MLLA calculations being already shown on Figs. 3 and 5, Fig. 25 displays, on the left, a “modified” MLLA calculation obtained by dividing by $\alpha_s(k_\perp^2) \approx \frac{\pi}{2N_c\beta y}$ (see (47) with $\lambda \rightarrow 0$); subtracting in the MLLA calculations the dependence on k_\perp due to the running of $\alpha_s(k_\perp^2)$ allows a better comparison with DLA (with fixed α_s) by getting rid of the divergence when $k_\perp \rightarrow Q_0$.

On the right are plotted the DLA results for gluon jets, in which α_s has been fixed at the collision energy (it is thus very small). Since their normalizations are now different, only the *shapes* of the two types of curves must be compared; we indeed observe that the DLA growing of $\frac{d^2N}{d\ell_1 d \ln k_\perp}$ with k_\perp (or y_1) also occurs in the “modified” MLLA curves.

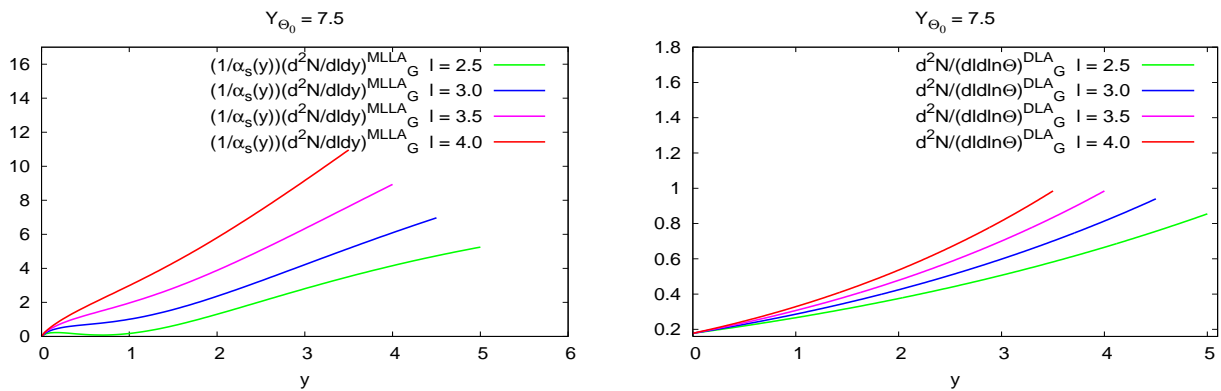


Fig. 25: comparison between MLLA (after dividing by $\alpha_s(k_\perp^2)$, on the left) and DLA calculation with α_s fixed (on the right) of $\frac{d^2N}{dy d \ln k_\perp}$ for gluon jets.

The DLA distribution for quark jets is obtained from that of gluon jets by multiplication by the factor C_F/N_c ; it is thus also a growing function of y_1 .

The MLLA distribution for quark jets, which is, unlike that for gluon jets, a decreasing function of y_1 (see Fig. 6), becomes, like the latter, growing, after the dependence on $\alpha_s(k_\perp^2)$ has been factored out: one finds the same behavior as in DLA.

E.3 Inclusive k_\perp distribution

On Fig. 26 we have plotted, at $Y_{\Theta_0} = 7.5$:

- the MLLA calculation of $\frac{dN}{d\ln k_\perp}$ divided by $\alpha_s(k_\perp^2)$, such that the divergence due to the running of α_s has been factored out, leaving unperturbed the damping due to coherence effects;
- the DLA calculation of $\frac{dN}{d\ln k_\perp}$ with α_s fixed at the collision energy.

Like in E.2, because of the division by α_s , the two curves are not normalized alike, such that only their *shapes* should be compared.

The comparison of the DLA curve (at fixed α_s) with the genuine MLLA calculation displayed in Fig. 7 (left) shows how different are the outputs of the two approximations; while at large k_\perp they are both decreasing, at small k_\perp the running of α_s makes the sole MLLA distribution diverge when $k_\perp \rightarrow Q_0$ (non-perturbative domain).

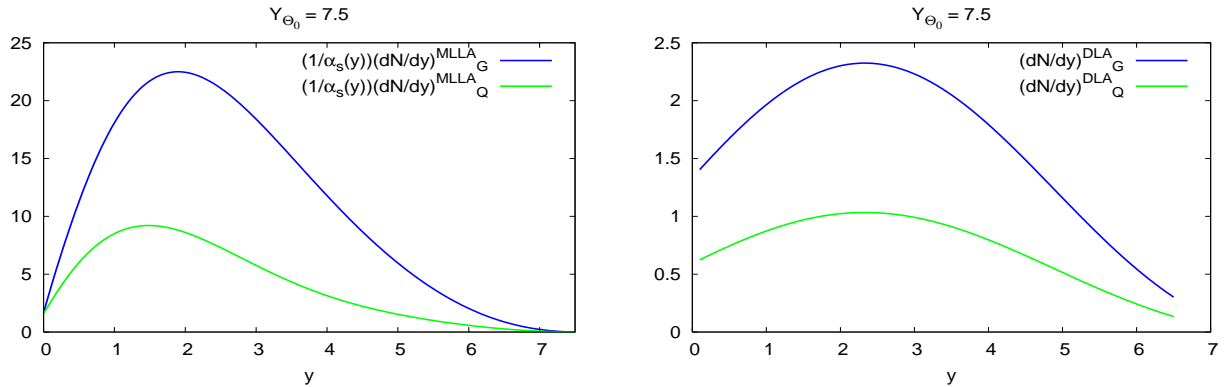


Fig. 26: $Y_{\Theta_0} = 7.5$: comparing MLLA and DLA calculations of $\frac{dN}{d\ln k_\perp}$ (see also Fig. 7); from left to right: $\frac{1}{\alpha_s(k_\perp^2)}$ MLLA and DLA (α_s fixed).

In the extremely high domain of energy $Y_{\Theta_0} = 15$ used for Fig. 27, the two competing phenomena occurring at small y_1 can then be neatly distinguished.

The first plot, showing MLLA results, cleanly separates coherence effects from the running of α_s ; in the second figure we have plotted the MLLA calculation divided by $\alpha_s(k_\perp^2)$: damping at small y_1 due to coherence effects appears now unspoiled; finally, DLA calculations clearly exhibit, too, the damping due to coherence ¹².

The large difference of magnitude observed between the first (genuine MLLA) and the last (DLA) plots occurs because DLA calculations have been performed with α_s fixed at the very high collision energy.

Like in E.2, because of the division by α_s , the second curve is not normalized like the two others, such that only its *shape* should be compared with theirs.

¹²The DLA points corresponding to $y_1 = 0$ can be analytically determined to be $4N_c/n_f$ (gluon jet) and $4C_F/n_f$ (quark jet); they are independent of the energy Y_{Θ_0} .

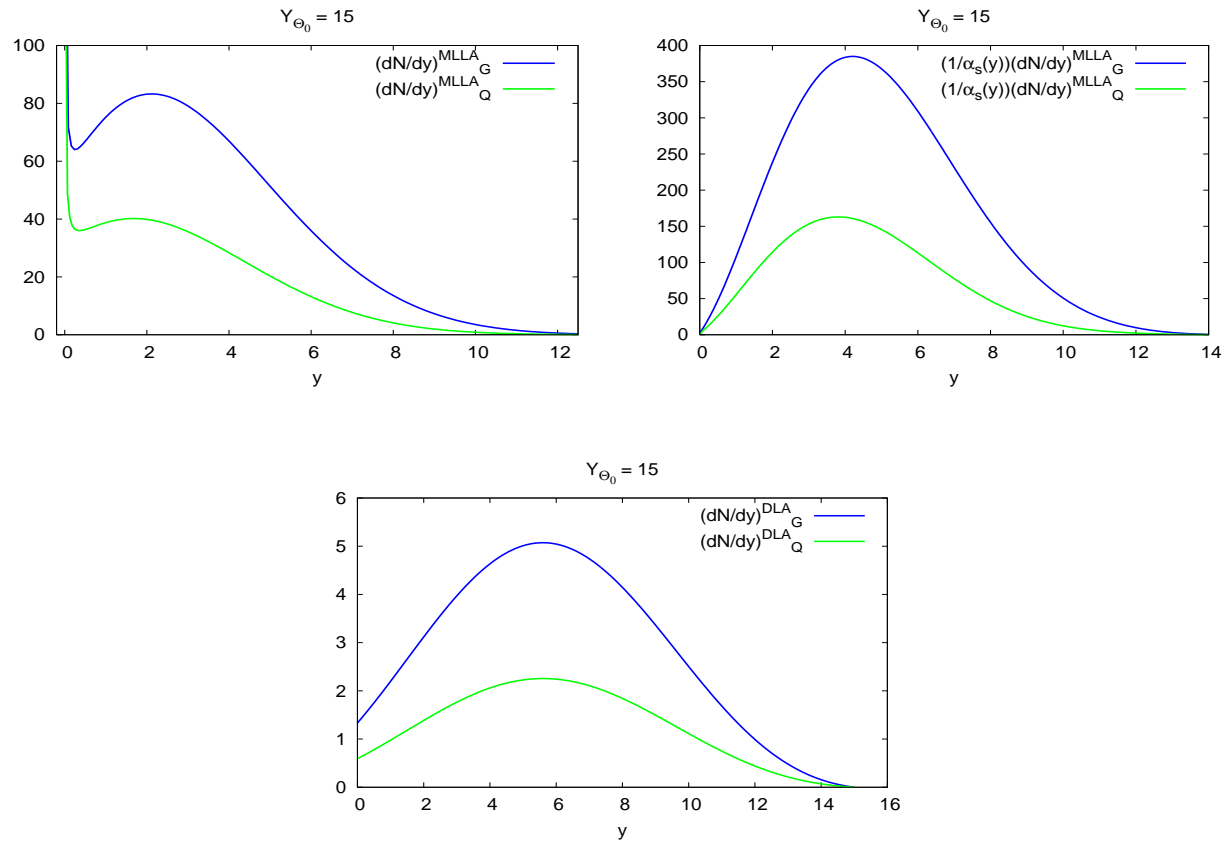


Fig. 27: $Y_{\Theta_0} = 15$: comparing MLLA and DLA calculations of $\frac{dN}{d \ln k_\perp}$;
 from left to right: MLLA, $\frac{1}{\alpha_s(k_T^2)}$ MLLA and DLA (α_s fixed).

Figure captions

Fig. 1: the process under consideration: two hadrons h_1 and h_2 inside one jet;

Fig. 2: $\langle C \rangle_{A_0}^0$ and $\langle C \rangle_{A_0}^0 + \delta \langle C \rangle_{A_0}$ for quark and gluon jets, as functions of y , for $Y_{\Theta_0} = 7.5$, $\ell = 2.5$ and $\ell = 3.5$;

Fig. 3: $\frac{d^2N}{d\ell_1 d\ln k_\perp}$ for a gluon jet, $Y_{\Theta_0} = 7.5$ and $Y_{\Theta_0} = 10$;

Fig. 4: $\frac{d^2N}{d\ell_1 d\ln k_\perp}$ at fixed ℓ_1 for a gluon jet, comparison between MLLA and the naive approach;

Fig. 5: $\frac{d^2N}{d\ell_1 d\ln k_\perp}$ for a quark jet, $Y_{\Theta_0} = 7.5$ and $Y_{\Theta_0} = 10$;

Fig. 6: $\frac{d^2N}{d\ell_1 d\ln k_\perp}$ at fixed ℓ_1 for a quark jet, comparison between MLLA and the naive approach;

Fig. 7: inclusive k_\perp distribution $\frac{dN}{d\ln k_\perp}$ for a gluon jet, $Y_{\Theta_0} = 7.5$ and $Y_{\Theta_0} = 10$, MLLA and naive approach, both for $\ell_{min} = 0$;

Fig. 8: enlargements of Fig. 6 at large k_\perp ;

Fig. 9: inclusive k_\perp distribution $\frac{dN}{d\ln k_\perp}$ for a quark jet, $Y_{\Theta_0} = 7.5$ and $Y_{\Theta_0} = 10$, MLLA and naive approach, both for $\ell_{min} = 0$;

Fig. 10: enlargements of Fig. 8 at large k_\perp ;

Fig. 11: role of the upper limit of integration over x_1 in the inclusive k_\perp distribution $\frac{dN}{d\ln k_\perp}$ for gluon (left) and quark (right) jet;

Fig. 12: spectrum $\tilde{D}_g(\ell, y)$ of emitted partons as functions of transverse momentum (left) and energy (right);

Fig. 13: enlargements of Fig. 11 close to the origin;

Fig. 14: $\frac{d\tilde{D}_g(\ell, y)}{dy}$ as a function of y for different values of ℓ ;

Fig. 15: $\frac{d\tilde{D}_g(\ell, y)}{dy}$ as a function of ℓ for different values of y ;

Fig. 16: $\frac{d\tilde{D}_g(\ell, y)}{d\ell}$ as a function of ℓ for different values of y ;

Fig. 17: $\frac{d\tilde{D}_g(\ell, y)}{d\ell}$ as a function of y for different values of ℓ ;

Fig. 18: $\langle C \rangle_{A_0}^0$ and $\langle C \rangle_{A_0}^0 + \delta \langle C \rangle_{A_0}$ for quark and gluon jets, as functions of y , for $Y_{\Theta_0} = 5.2$, $\ell = 1.5$ and $\ell = 2.5$;

Fig. 19: $\frac{d^2N}{d\ell_1 d\ln k_\perp}$ for a gluon jet for $Y_{\Theta_0} = 5.2$ at fixed ℓ_1 , MLLA and naive approach;

Fig. 20: $\frac{d^2N}{d\ell_1 d\ln k_\perp}$ for a quark jet for $Y_{\Theta_0} = 5.2$ at fixed ℓ_1 , MLLA and naive approach;

Fig. 21: $\frac{dN}{d\ln k_\perp}$ for a gluon jet for $Y_{\Theta_0} = 5.2$, MLLA and naive approach;

Fig. 22: $\frac{dN}{d\ln k_\perp}$ for a quark jet for $Y_{\Theta_0} = 5.2$, MLLA and naive approach;

Fig. 23: $\frac{dN}{d\ln k_\perp}$ for a gluon and a quark jets, MLLA predictions for the Tevatron.

Fig. 24: the spectrum $\tilde{D}_g(\ell, Y_{\Theta_0} - \ell)$ for gluon jets; comparison between MLLA and DLA (“with running α_s ”) calculations;

Fig. 25: comparison between MLLA (after dividing by $\alpha_s(k_\perp^2)$, on the left) and DLA calculation with α_s fixed (on the right) of $\frac{d^2N}{dy d\ln k_\perp}$ for gluon jets;

Fig. 26: $Y_{\Theta_0} = 7.5$: comparing MLLA and DLA calculations of $\frac{dN}{d \ln k_\perp}$ (see also Fig. 6); from left to right: $\frac{1}{\alpha_s(k_T^2)}$ MLLA and DLA (α_s fixed);

Fig. 27: $Y_{\Theta_0} = 15$: comparing MLLA and DLA calculations of $\frac{dN}{d \ln k_\perp}$; from left to right: MLLA, $\frac{1}{\alpha_s(k_T^2)}$ MLLA and DLA (α_s fixed).

References

- [1] Yu.L. Dokshitzer, V.A. Khoze, A.H. Mueller and S.I. Troyan: “*Basics of Perturbative QCD*” (Editions Frontières, Paris, 1991), and references therein.
- [2] C.P. Fong and B.R. Webber: Phys. Lett. **B 229** (1989) 289.
- [3] OPAL Collab., M.Z. Akrawy et al.: Phys. Lett. **B 247** (1990) 617-628.
JADE Collab. and OPAL Collab., P. Pfeifenschneider et al.: Eur. Phys. J. **C 17** (2000) 19-51.
- [4] CDF Collab., T. Affolder et al.: Phys. Rev. Lett. **87** (2001) 211804;
CDF Collab., D. Acosta et al.: Phys. Rev. **D 68** (2003) 012003.
- [5] H1 Collab., C. Adloff et al.: Eur. Phys. J. **C 21** (2001) 33-61;
H1 Collab., C. Adloff et al.: Phys. Lett. **B 542** (2002) 193.
- [6] Yu.L. Dokshitzer, V.A. Khoze, S.I. Troyan and A.H. Mueller: Rev. Mod. Phys. **60** (1988) 373-388.
- [7] V.A. Khoze and W. Ochs: Int. J. Mod. Phys. **A12** (1997) 2949.
- [8] R. Perez Ramos: “*Two particle correlations in QCD jets*”, *to appear*.
- [9] R. Perez Ramos: “*Correlations between two particle in jets*”, in “QCD and High Energy Hadronic Interactions”, Proceedings of “Rencontres de Moriond” (La Thuile, March 12-19th 2005), THE GIOI Publishers, E. Auger & J. Tran Thanh Van, editors, p. 197.
- [10] Yu.L. Dokshitzer, D.I. Dyakonov and S.I. Troyan: “*Inelastic processes in Quantum Chromodynamics*”, SLAC-TRANS-183, translated from Proceedings of 13th Leningrad Winter School (1978), 1-89;
Yu.L. Dokshitzer, D.I. Dyakonov and S.I. Troyan: “*Hard processes in Quantum Chromodynamics*”, Phys. Rept. **58** (1980) 269-395.
- [11] Yu.L. Dokshitzer and D.I. Dyakonov: “*Quantum Chromodynamics and hadron jets*”, DESY-L-TRANS-234 (Jul. 1979). Translated from Proceedings of 14th Leningrad Winter School (1979) p. 27-108 (translation).
- [12] H.D. Politzer: Phys. Rep. **14 C** (1974) 130.
- [13] V.N. Gribov and L.N. Lipatov: Sov. J. Nucl. Phys. **15** (1972) 438 and 675;
L.N. Lipatov: Sov. J. Nucl. Phys. **20** (1975) 94;
A.P. Bukhvostov, L.N. Lipatov and N.P. Popov: Sov. J. Nucl. Phys. **20** (1975) 286;
G. Altarelli and G. Parisi: Nucl. Phys. **B 126** (1977) 298;
Yu.L. Dokshitzer: Sov. Phys. JETP **46** (1977) 641.
- [14] Yu.L. Dokshitzer, V.S. Fadin and V.A. Khoze: Z. Phys. **C18** (1983) 37.
- [15] Yu.L. Dokshitzer, V.S. Fadin and V.A. Khoze: Phys. Lett. **B 115** (1982) 242.
- [16] R. Perez-Ramos & G.P. Salam: in preparation.
- [17] I.S. Gradshteyn and I.M. Ryzhik: “*Table of Integrals, Series, and Products*” (Academic Press, New York and London, 1965).

[18] L.J. Slater, D. Lit (Ph.D): “*Confluent Hypergeometric Functions*”, Cambridge University Press (London, New-York) 1960.

Kt distribution

